KAGRA Instrument Science White Paper 2024

KAGRA Future Strategy Committee

December 27, 2024

JGW-T2416182, Overleaf link

1 Executive Summary

We reviewed over 60 technologies that could potentially be implemented to upgrade KAGRA, evaluating their feasibility on a scale from 0 to 5 according to the criteria detailed in Sec. 3. Each technology was also rated for its relevance to improving low-frequency sensitivity, high-frequency sensitivity, broadband sensitivity, stability, and accuracy, with a score from 0 to 2. A relevance score of 0 indicates minimal or no relevance, 1 indicates moderate relevance, and 2 indicates high relevance or necessity.

To determine the readiness, the feasibility score was multiplied by the relevance score, and we calculated the average of the products for relevance scores of 1–2. This resulted in an average product score of **2.90 for low-frequency, 4.38 for high-frequency, and 3.22 for broadband improvements**. A detailed score table can be found in the last two pages of this section and Google spreadsheet in this link. The overall trend was consistent with the technology scores summarized in the 2019 FPC White Paper [JGW-M1909590].

In addition, we analyzed various example upgrade plans in Sec. 4 to identify the research and development efforts necessary to enhance KAGRA's sensitivity. The high-priority development items are as follows:

- High Q-factor sapphire fibers and blade springs. Blade springs with lower resonant frequencies.
- Large, uniform and low absorption sapphire mirrors.
- Output optics and filter cavity with low optical losses. Technologies to reduce mode-matching losses.
- Technologies for higher power operations.
- Control schemes for higher finesse signal recycling cavity and arm cavities.

Technology Survey 2024	Feasibility	Relevance				
		LF	HF	BB	Stability	Accuracy
Average Feasibility x Relevance		**2.90**	**4.38**	**3.22**	**2.78**	**4.00**
High power laser	3	0	2	1		
Use of different wavelengths	3	1	1	1		
Multi-carrier injection	0	1	1	1		
Frequency-independent squeezing	5	0	2	0		
Frequency-dependent squeezing	5	1	0	2		
Birefringence compensation	2	0	1	1	1	
Large beam	3	0	0	2		
Large sapphire mass	2	2	0	2		
Silicon test mass	1	1	0	1		
Use of different materials for substrate	0	1	0	1		
Composite mass	0	1	0	1		
Parametric instability mitigation	5	0	2	1	1	
Thermal compensation system	5	0	2	1		
Use of different materials for coating	2	0	0	2		
Non-TEM00 beam	3	0	0	1		
Non-cylindrical mass	0	1	0	1		
Khalili cavity	1	0	0	1		
Gratings	2	0	0	1		
Radiative cooling		1	0	1		
Reducing vibration of cryogenic components	3.5	2	0	0		
Sapphire blade spring improvement	2	2	0	1		
Use of ribbons	2	1	0	1		
Use of long fibers	1	2	0	1		
High conductivity fibers		1	2	1		
Large beam splitter	5	0	1	1		
Low-loss Faraday isolator	5	0	2	2		
Low-loss OMC	5	0	2	2		
Low-loss PD	3	0	2	2		
Adaptive control for better seismic isolation	4	2	0	0	1	
Better damping control	4	2	0	0	1	
Low-frequency vibration isolation	3	2	0	0		
Suspension point interferometer	3	1	0	0	1	
Vertical suspension point interferometer	0	1	0	0		
Newtonian noise studies and cancellation	2	2	0	0	1	
Environmental magnetic noise sensors	5	1	0	0		
Charge noise reduction	0	1	0	0		
Instrumented baffles	3	1	0	0		
Schumann resonance	5	1	0	0		
Thermal noise in non-equilibrium steady state	3	1	0	0		
Gravitational decoherence noise	0	0	0	0		
Phase camera	5	1	0	1		
Machine learning	5	1	1	1	1	1
Noise subtraction methods	5	2	1	1		

Laser induced desorption	0	0	1	1		
Quantum locking	3	1	0	0		
Homodyne readout	3	1	0	2		
Variational readout	2	1	0	1		
Optical spring	4	1	0	0		
Long-SRC	3	0	2	0		
Quantum expander	2	0	1	1		
Intracavity OPA	3	0	1	0		
White-light cavity	2	0	1	0		
PT symmetry	2	0	1	0		
Kerr amplification	2	0	1	0		
Photo-thermal effect	2	1	1	0		
EPR squeezing	3	1	0	1		
Quantum teleportation	1	1	0	1		
Negative effective mass	1	1	0	1		
Speed-meter	1	1	0	0		
Acceleration-meter	1	1	0	0		
Negative intertia	1	1	0	0		
Local readout	1	1	0	0		
Photon counting	2	0	1	0		
Delay line	4	0	0	1		
Displacement noise free interferometer	1	0	0	0		
L resonator	2	0	1	0		
Multi-color calibration	3	0	0	0		1
Tidal compensation using geophysics interferometer		0	0	0	1	
Earthquake monitors		0	0	0	1	

Contents

2 Introduction

In 2019, KAGRA Future Planning Committee [wiki page] wrote KAGRA FPC White Paper [JGW-M1909590], which summarized the science cases and technologies for potential KAGRA upgrade plans. It also contained an overview of bKAGRA design sensitivity [JGW-T1707038] and technical design. The result of the extensive science case study was published as PTEP 2021, 05A103 (2021), and the summary of potential KAGRA upgrade plans was published as PRD 102, 022008 (2020). Then in 2021, KAGRA Future Strategy Committee was formulated to further organize activities for future upgrade of KAGRA.

Since 2019 version of the white paper, no major update was done. From 2024, we decided to update the white paper yearly, focusing on survey of current technologies. For each technology, description will be updated yearly when there is some progress related to that technology. We will not include the science case part and the overview of bKAGRA, as we can refer to LVK Observational Science White Paper [LIGO-T2300406] and the FPC white paper.

In the current LVK observing plan, O5 is expected in mid-2027 to mid-2030 [webpage], with a target sensitivity of 25 to 128 Mpc. This FSC White Paper focuses on upgrades happening after O5 and beyond, but also discusses possible upgrades that can be implemented before O5. Technologies covered in this white paper include those for improving the sensitivity, stability, and calibration accuracy.

The rest of the white paper is organized as follows. Section 3 summarizes the survey of current technologies relevant for upgrading KAGRA. In Section 4, possible upgrade plans combining these technologies are discussed, and some of the representative plans are compared based on basic figure of merits. Section 1 is an executive summary of the white paper, which includes a summary table for the feasibility and the relevance for upgrading KAGRA for each technology, and a summary of R&D necessary for upgrading KAGRA.

We hope that this white paper stimulates science case discussions and shows future directions for R&D activities for upgrading KAGRA.

References:

- KAGRA Future Planning Committee, *KAGRA FPC White Paper - Part I*, JGW-M1909590.
- Y. Enomoto, K. Komori, Y. Michimura, K. Somiya, K. Yamamoto, T. Yamamoto, *Latest estimated sensitivity of KAGRA (v201708)*, JGW-T1707038.
- KAGRA Collaboration, Progress of Theoretical and Experimental Physics 2021, 05A103 (2021).
- Y. Michimura *et al.*, Physical Review D 102, 022008 (2020).
- *LIGO, Virgo and KAGRA Observing Plans*, https://observing.docs.ligo.org/plan/.

3 Survey of Current Technologies

In this section, we review various technologies that could be implemented in KAGRA. Technologies those might not be feasible in the near future are also reviewed. Feasibility of each technology is scored from 0 to 5 under the following criteria with a short description to justify:

- 0: Idea phase
- 1: Theoretically well studied
- 2: Demonstration experiment on going
- 3: Demonstrated with a table-top experiment
- 4: Demonstrated with a prototype experiment (e.g. TAMA)
- 5: Demonstrated with one of LVK detectors

The review texts were copied from the 2019 version of the FPC White Paper when they are available, and updated to reflect recent progress or summarized to shorten the text. Updates are highlighted in red. For technologies those were not in 2019, the text is always not highlighted. Version history was also written to keep track of each review text.

3.1 Light sources

3.1.1 High power laser

Version history: First version in 2019 by S. Haino; Summarized in October 2024 by Y. Michimura
Feasibility: 3 (Some demonstrations at table-top scale are done.)

Ultra-stable high-power laser systems are essential components of the interferometric GW detectors. For 1064 nm in LIGO, a new configuration is

considered with 35 W front end system followed by two neoVAN 4S-HP amplifiers in series to achieve 170 W power at TEM_{00} [LIGO-L1800375]. This would be one of the most feasible options to achieve the high power laser by using the solid state amplifiers.

The current generation GW detectors require about 150 W of single-frequency laser power, while the future detector design may require up to the order of 500 W. Single-frequency fiber lasers for 1–3 μm have recently drawn intense attention, and output powers of a few hundred Watts have been demonstrated. See [Li 2023] and Fig. 1 for a review. Since the 2019 White Paper, output power record for 1064 nm increased from 414 W to 703 W. Not only the output power but also the noise performances still need to be investigated.

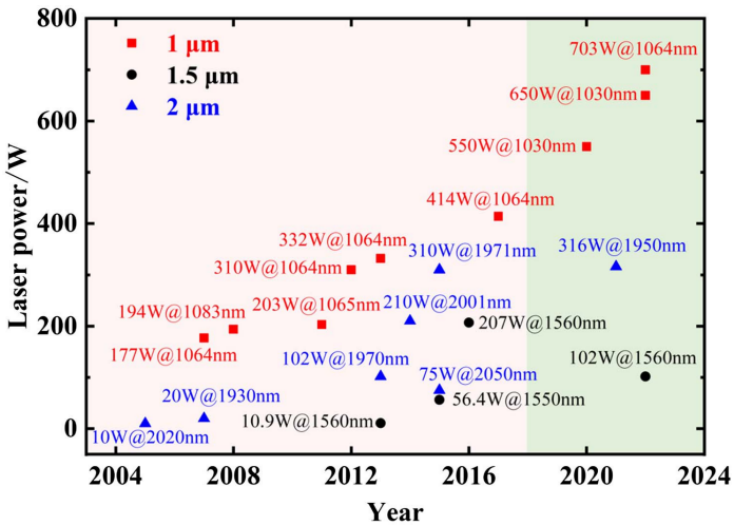

Figure 1: Output power evolution of CW single-frequency amplifiers in all-fiber format operating in 1, 1.5, and 2 μm regions [Li 2023].

References:

- P. Fritschel *et al.*, LIGO-L1800375 (2018).
- C. Li *et al.*, Chin. Opt. Lett. 21, 090002 (2023).

3.1.2 Use of different wavelengths

Version history: First version in October 2024 by Y. Michimura
Feasibility: 3 (Some demonstrations at table-top scale are done.)

Use of laser wavelengths other than 1064 nm would be necessary for silicon interferometer. There are also possibilities of using different wavelengths even if we stick to fused silica optics. Availability of high power laser sources in 1–2 um are given in Section 3.1.1.

The quantum efficiency for 1550 nm is very high (QE > 99%) in standard InGaAs photodiodes [Mehmet 2011]. The quantum efficiency of InGaAs for longer wavelengths can be tuned by adjusting the In/Ga ratio. However, this leads a greatly increased dark noise level [LIGO-T1900380]. One possibility to effectively increase the quantum efficiency is to downconvert the signal light into lower laser wavelengths using sum frequency generation [LIGO-T1400226].

Squeezing amplitude of 11.5 dB from 10 kHz down to below 1 Hz has been demonstrated at 1550 nm [Meylahn 2022]. Squeezing amplitude of 4 dB at kHz region at 1984 nm [Mansell 2018], and 7.2 dB at MHz region at 2128 nm has been demonstrated [Darsow-Fromm 2021]. Considering the history of squeezing developments for 1064 nm, it is expected that 10–15 dB of squeezing can be achieved.

References:

- M. Mehmet *et al.*, Optics Express 19, 25763 (2011).
- S. Singh *et al.*, LIGO-T1900380 (2019).
- R.X. Adhikari *et al.*, LIGO-T1400226-v10 (2024); See Sec. 9.3.3.
- F. Meylahn *et al.*, Phys. Rev. Lett. 129, 121103 (2022).
- G. L. Mansell *et al.*, Phys. Rev. Lett. 120, 203603 (2018).
- C. Darsow-Fromm *et al.*, Optics Letters 46, 5850 (2021).

3.1.3 Multi-carrier injection

Version history: First version in 2024 by K.Somiya
Feasibility: 0

This is an idea to use multiple laser fields to optimize the quantum noise spectrum. One simple example is to add a secondary carrier with lower power and lower finesse than the primary field so that total radiation pressure noise does not change much while shot noise sensitivity with the secondary carrier is better than the primary.

The local readout scheme 3.10.4 is another example of the multi-carrier injection. The double optical spring 3.9.3 is based on a different concept but it can be regarded as one of the multi-carrier injection schemes.

3.1.4 Frequency-independent squeezing

Version history: First version in 2019 version (JGW-M1909590) ; Updated in July 2024 by R.-K. Lee
Feasibility: 5 (GEO, TAMA, Virgo, and LIGO had implemented FIS and FDS)

Frequency independent squeezing (FIS) is necessary to reduce quantum noises, as well as the first step to implement FDS and EPR Squeezing.

For 1064nm, production of FIS is a mature technique and it is currently applied to second generation interferometers to reduce shot noise, demonstrated

in GEO, TAMA, Virgo, and LIGO. Even though up to 15dB of squeezing has demonstrated in the MHz region, [Vahlbruch *et al.*2016]; in the frequency band from 10 Hz to 100 kHz, only up to 12dB of squeezing was realized by AEI group [Mehmet *et al.*2019].

Within the KAGRA collaboration, the filter cavity experiment team in TAMA has developed FIS source (as well as FDS) with a maximum squeezing level of 6.1dB below shot noise (and 15.9 dB of antisqueezing) down to 10 Hz from a linear hemilithic cavity hosting a periodically poled potassium titanyl phosphate (PPKTP) crystal [Zhao *et al.*2020]. At present, a new designed bow-tie cavity from National Tsing Hua University (NTHU), Hsinchu, Taiwan, is measured at NAOJ with 5.6dB squeezing (and 17.7db antisqueezing) in the MHz region and under test for low frequency region.

For 1550nm, squeezed light with a quantum noise reduction of 12.3 dB was reported at 5 MHz, and approximately 5dB at 2kHz [Mehmet *et al.*2011]. But there has not yet significant result for low frequency region.

In order to extract the degradation of squeezing light source, machine-learning enhanced quantum state tomography has implemented in NTHU [Hsieh *et al.*2022], and applied to TAMA. Deployment of machine-learning to FPGA is also tested for the potential real-time diagnosis toolbox for KAGRA.

With the target of 10dB squeezing, phase noise is the current bottleneck. How to reduce the antisqueezing, keeping the purity of FIS, needs to some studies.

References:

- M. Mehmet and H. Vahlbruch, "High-efficiency squeezed light generation for gravitational wave detectors," Class. Quant. Grav. 36, 015014 (2019).
- H. Vahlbruch et al., "Detection of 15 dB Squeezed States of Light and their Application for the Absolute Calibration of Photoelectric Quantum Efficiency," Phys. Rev. Lett. 117, 110801 (2016).
- Y. Zhao et al., "Frequency-Dependent Squeezed Vacuum Source for Broadband Quantum Noise Reduction in Advanced Gravitational-Wave Detectors," Phys. Rev. Lett. 124, 171101 (2020).
- Virgo Collaboration, "Frequency-Dependent Squeezed Vacuum Source for the Advanced Virgo Gravitational-Wave Detector," Phys. Rev. Lett. 131, 041403 (2023).
- LIGO O4 Detector Collaboration, "Broadband Quantum Enhancement of the LIGO Detectors with Frequency-Dependent Squeezing," Physical Review X 13, 041021 (2023).
- M. Mehmet et al., "Squeezed light at 1550 nm with a quantum noise reduction of 12.3 dB," Optics Express 19, 25763 (2011).
- H.-Y. Hsieh et al., "Extract the Degradation Information in Squeezed States with Machine Learning," Phys. Rev. Lett. 128, 073604 (2022).

3.1.5 Frequency-dependent squeezing

Version history: First version in 2019 version (JGW-M1909590) ; Updated in October 2024 by M. Page
Feasibility: 5 (LIGO and Virgo have implemented frequency dependent squeezing using 300 m filter cavities similar to the TAMA prototype)

Frequency dependent squeezing (FDS) for 1064 nm carriers is a mature technique that has been implemented into the LIGO and Virgo detectors. Frequency independent squeezing was used in LIGO to achieve 3 dB of quantum shot noise reduction at high frequency. However, the associated appearance of quantum radiation pressure noise at low frequency meant that further squeezing improvement required a broadband approach. A very long filter cavity is used to rotate the squeezed quadrature to align with the noise response of the interferometer, resulting in broadband quantum noise reduction [H. Kimble *et al.*(2001)]. Hanford, Livingston and Virgo all use 300m filter cavities. After the construction of the filter cavities and the completion of O4 commissioning, LIGO Hanford demonstrated a peak quantum noise reduction of 4 dB at around 1 kHz, while Virgo and LIGO Livingston reached almost 6 dB [D. Ganapathy *et al.*(2023)][F. Acernese *et al.*(2023)]. Space constraints within the Kamioka mine restrict a potential KAGRA filter cavity to 85 m length.

Within the KAGRA collaboration, the filter cavity experiment at TAMA [Y. Zhao *et al.*(2020)] initially showed 3 dB of shot noise squeezing above the ellipse rotation frequency and 1.4 dB of radiation pressure squeezing down to approximately 60 Hz. The noise spectrum at less than 50 Hz was strongly limited by spurious light coupling to filter cavity residual motion. The leading cause of general squeezing degradation was optical loss from propagation optics, sub-optimal escape efficiency of the optical parametric oscillator and mode mismatch to the filter cavity.

In FDS, performance of the vacuum Faraday isolator is critical, since it helps to reduce spurious light reaching the filter cavity. However, it also introduces relatively large optical loss compared to other propagation optics. For TAMA, the leading source of squeezing degradation in the vacuum envelope is from the Faraday isolator, which is the original Faraday isolator from the TAMA gravitational wave detector. KASI have developed an improved in-vacuum Faraday isolator with reduced optical loss, 40 dB of isolation and a more modern design with increased flexibility.

One of the technical difficulties in FDS is control of the filter cavity length and alignment, which must be performed with a bright probe offset from the carrier (squeezing) frequency to avoid scattered light contamination of the squeezing. The initial demonstration in TAMA used a pick-off from the squeezer green pump. In principle, the filter cavity is simultaneously resonant for the green pump pick-off and the squeezed vacuum, however, refractive index dispersion of the mirror and nonuniformity of the coating causes a slight offset of the resonant conditions for the first and second harmonics. The TAMA team later demonstrated auto-alignment using green and highlighted some mitigation issues for the tuning offset between the first and second harmonics [Y. Zhao *et*

al.(2022)]. Virgo implemented the same locking scheme in their filter cavity for O4 [F. Acernese *et al.*(2023)].

Optimally, the filter cavity should be controlled using a co-propagating detuned infrared beam. There are three different approaches in the FDS designs of LIGO, Virgo and KAGRA. In LIGO, the infrared control field is generated by modulating the main laser using a double AOM scheme. The Virgo design proposed to use an independent laser unit aligned and mode matched to the OPO. While this is not inherently co-propagating, it has the advantage of high signal-to-noise ratio and phase stability for the control field. In TAMA, infrared control was achieved by injecting a detuned field into the OPO as an upper sideband of the squeezed frequency. Nonlinear interaction then generates a lower infrared sideband which is mode matched and co-propagating with squeezing [N. Aritomi *et al.*(2022)].

References:

- LIGO O4 Detector Collaboration, "Broadband Quantum Enhancement of the LIGO Detectors with Frequency-Dependent Squeezing," Physical Review X 13, 041021 (2023).
- Virgo Collaboration, "Frequency-Dependent Squeezed Vacuum Source for the Advanced Virgo Gravitational-Wave Detector," Phys. Rev. Lett. 131, 041403 (2023).
- Y. Zhao et al., "Frequency-Dependent Squeezed Vacuum Source for Broadband Quantum Noise Reduction in Advanced Gravitational-Wave Detectors," Phys. Rev. Lett. 124, 171101 (2020).
- Y. Zhao et al., "Improving the stability of frequency dependent squeezing with bichromatic control of filter cavity length, alignment and incident beam pointing," Phys. Rev. D 105, 082003 (2022)
- N. Aritomi *et al.*"Demonstration of length control for a filter cavity with coherent control sidebands," Phys. Rev. D 106, 102003 (2022)
- H.-Y. Hsieh et al., "Extract the Degradation Information in Squeezed States with Machine Learning," Phys. Rev. Lett. 128, 073604 (2022).

3.2 Test masses and coatings

3.2.1 Birefringence Compensation

Version history: First version in August 2024 by M. Eisenmann and S. Singh
Feasibility: 2 (M. Eisenmann, S. Singh demonstrated with a table-top in 1D 2024)

A pair of tunable polarization retarders can generate any polarization states. The pair can compensate the birefringence of KAGRA Input Test-Masses. This will reduce the induced depolarization effect.

A demonstration of birefringence compensation of a 23 kg sapphire is shown in figure 2. It is achieved using a pair of liquid crystal cells with their fast-axis

oriented at 45° relative to each other. The tuning of their voltages can recover the input polarization. A reduction by a factor of 10^5 was achieved for both the polarization rotation and retardation [Eisenmann *et al.*2024].

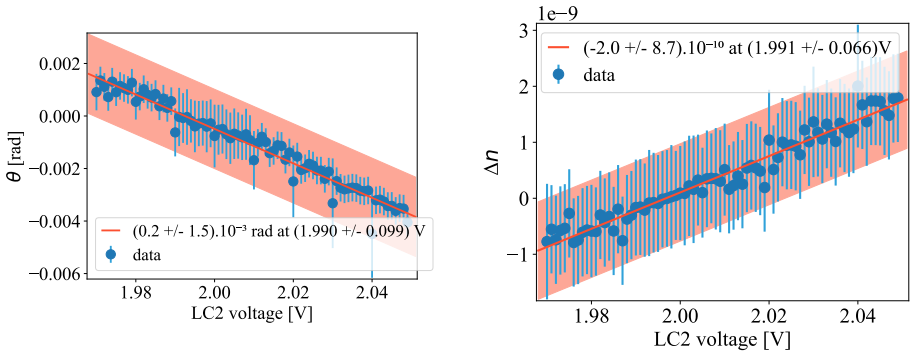

Figure 2: Reduction of the birefringence of a 23 kg Sapphire by tuning the second liquid crystal voltage.

The LC used was from Thorlabs and had a transmission of 98%. Although the tabletop experiment used a lossy variable retarder, it can compensate for the birefringence effect on alignment control beams (the output of IFO) with reduced requirements for optical loss. However, to establish a 2D compensation system before the test mass, several challenges must be addressed to meet the requirements for future upgrades. We must address factors from 2D actuation to low-loss solutions while avoiding introducing new noises. The birefringence compensation system can potentially resolve the problems caused by inhomogeneity in test-mass birefringence. This project has a huge potential to explore new possibilities and mitigate non-uniform birefringence using thermal compensation techniques with the help of a favorable thermo-optic material.

References:

- M. Eisenmann, S. Singh, M. Leonardi, Opt. Lett. 49, 3404-3407 (2024).

3.2.2 Large beam

Version history: First version in 2024 by H. Wang.
Feasibility: 3 (H. Wang demonstrated with a table-top in 2018)

The design peak sensitivity around Fourier frequencies of 100 Hz of the current (second) generation of gravitational wave detectors is limited by thermal noise, in particular, the coating Brownian noise. Different methods have been proposed to reduce this thermal noise: cryogenic cooling of the test masses, new coating materials with decreased mechanical losses, optimisation of coating thickness, all-reflective interferometers, larger beam spot size on test masses or higher-order spatial laser beam modes.

Using larger beam spot size on cavity mirrors can provide a reduction in coating thermal noise [Hong *et al.*2013]. There are, however, two factors at play

limiting the maximum beam size: the available mirror size and the stability of the cavity. The mirror size is usually determined by the available substrate size and maximum coated area. An empirical ratio of mirror radius to beam radius is 2.5, in which the clipping loss is only a few ppm (parts per million) [Hild 2010]. Another concern with using large beam sizes lies on the stability of the cavity, which can easily become critical. Using longer arm cavities would certainly help in achieving larger beam sizes whilst maintaining stability, but the cavity length is limited in ground-based detectors. Using large beam sizes thus requires pushing the cavity parameters towards the edge of geometric stability which is defined by the *g-factor*.

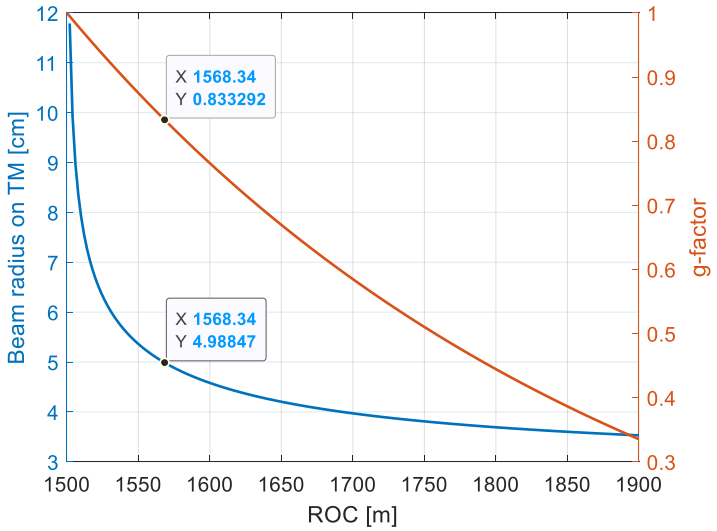

Figure 3: Beam size (radius) and g-factor as a function of the ROC of test masses.

The g-factor of current KAGRA arm cavities is: $g_c = g_1 g_2 = (1 - L/ROC)^2 = 0.34$, where L is the cavity length and ROC is the radius of curvature of the test mass of the symmetric cavity. Since the cavity stability is far away from the edge (where $g_c = 0$ or $g_c = 1$), it is possible that we use lager beam spot size by changing the cavity configuration. Figure 3 shows the beam radius and g-factor as a function of the ROC of test masses. If we increase the g-factor to 0.83 (aLIGO case), the beam radius will be enlarged from 3.5cm to 5.0cm (42% improvement). We can further change the cavity configuration from symmetric one to asymmetric one (whilst keeping g-factor the same) where the beam spot on ETM is larger. This will provide additional reduction in the total coating thermal noise as the coating of ETM is much thicker than that of ITM.

The reason for KAGRA of using 1900 m ROC for test masses was because we used the reference optics of LIGO wihch has a ROC around 1900 m (ROC of the ITM is 1934 m). But Virgo test masses have ROCs of 1420 m (ITM) and

1683 m (ETM). If we use reference optics from Virgo, it is possible to increase the g-factor for KAGRA. Then the limiting factor for using larger beam size mainly comes from the available mirror size.

References:

- T. Hong *et al.*, Physical Review D **87**, 082001 (2013).
- H. Wang, Doctoral dissertation, University of Birmingham, 2017.
- H. Wang *et al.*, Physical Review D **97**, 022001 (2018).
- LIGO Scientific Collaboration, LIGO Document **T1600119** (2016).
- B. Barr *et al.*, LIGO Document **T1200046** (2012).
- S. Hild, LIGO Document **G1300577** (2013).
- S. Hild, LIGO Document **G1000715** (2010).

3.2.3 Large sapphire mass

Version history: First version in 2019 by S.H. with input from E. Hirose. Updated by M. Eisenmann in September 2024.

Feasibility: **2** (iLM/LMA is currently developing growth process of 30 cm diameter sapphire)

One of the most challenging tasks have been the fabrication and quality control of the Test-Masses (TMs) which are made of sapphire. In the original KAGRA design [K. Somiya *et al.*2012], maximum possible size was assumed as 25 cm diameter with 30 kg but it turned out that 22 cm diameter is the largest one with the C-axis crystal with optics quality and larger mirror could contain bubbles. Because of the hardness of sapphire it took about a year for the machining and it was the first time for the polish company to machine such a large size. Each sapphire crystal has own individual property and it could lead failure if we don't be careful ([E. Hirose 2018],[E. Hirose 2018]). One of the most challenging task was to produce a low heat absorption bulk crystal of sapphires, particularly for the ITMs. We asked to two companies to fabricate the sapphire bulk crystal (company A and B). Company A and B produced 8 and 12 bulks, respectively. We found two bulks which satisfies the requirements of less than 50 ppm/cm absorption [E. Hirose 2017]. These two bulks have been selected for ITMs. After company Bs No. 2 was produced, measured and selected for ITMX, we tried to re-produce No. 2 monitoring parameters in growth process but could not and a clue between those parameters and absorption at 1064 nm.

In addition, the ITMs birefringence appeared as an additional issue [H. Wang *et al.*2024]. Despite correlation between the absorption and birefringence at 1064 nm of 23 cm diameter sapphire substrates [S. Zeidler *et al.*2023], neither of their origin is currently understood, which hinders the quality improvement of large sapphire substrates. Nevertheless, reducing annealing at intermediate temperature (¿1100 degC) or under-vacuum high temperature annealing were

proven to reduce bulk's absorption by 50% [Route *et al.*2004]. The effect of such annealing on sapphire's birefringence was not investigated but could provide a path towards reduced birefringence. Furthermore, as KAGRA relies on industrial manufacturer for the growth of its sapphire bulk, there was no clear improvement in the sapphire optical quality between 2019 to 2024 at the exception of AZTEC's bulk grown along the a-axis that exhibited a more uniform birefringence [M. Eisenmann *et al.*2022]. Finally, the ILM and LMA are currently developing the growth of large sapphire bulk and could already demonstrate repeatable growth of 30 mm diameter sapphire with about around or below 50 ppm/cm and down to 10 ppm/cm [T. Aventin *et al.*2024]. By modifying the aspect-ratio of KAGRA TM towards thinner but larger diameter TMs, the effect of absorption and birefringence would be reduced while it would be possible to reduce the thermal noise by increasing the laser beam size. Currently, the largest possible TMs mass is limited to 40 kg due to cryostat and Type-A suspension constraints. Further increase (as planned for LIGO, Virgo, Einstein Telescope, Cosmic Voyager and Cosmic Explorer) would require a redesign of Type A suspension and the cryostat. This size increase would also require the development of new characterization apparatus able to measure bulk scattering, absorption and birefringence for sample's diameter of more than 23 cm without inducing stress on the sample.

References:

- K. Somiya *et al.*, Class. Quantum Grav. 29 124007 (2012).
- E. Hirose, JGW-G1808499 (2018).
- E. Hirose, JGW-G1809520 (2018).
- E. Hirose, JGW-G1706429 (2017).
- H. Wang *et al.*, preprint (2024).
- M. Eisenmann *et al.*, JGW-G2214259 (2012).
- S. Zeidler *et al.*, Scientific Reports vol 13, 21393 (2023).
- T. Aventin *et al.*, CrystEngComm (2024).

3.2.4 Silicon test masses

Version history: First version in 2019 by K. Komori, updated in October 2024 by Y. Michimura

Feasibility: 1 (Well studied for LIGO Voyager and ET, but not demonstrated)

Silicon is one of the promising materials for mirror substrates and suspension fibers for future gravitational wave detectors, and seriously considered in LIGO Voyager [Adhikari 2020, Adhikari 2024] and Einstein Telescope. This is because of excellent mechanical, thermal and optical properties at cryogenic temperatures. Silicon boules of more than 100 kg with required purity and optics at 1.5-2 um still need to be developed. There could be unexpected phase noise in

silicon, and demonstration plans such as Mariner 40 m and ET pathfinder are underway.

Measured mechanical Q factor of silicon bulk reached 10^8 at around 100 K and 10^9 below 10 K [McGuigan 1978]. Also, the thermal expansion of silicon is zero at 18 K and 124 K [Lyon 1977], and thermoelastic noise can be eliminated at these temperatures. Especially, the temperature of 124 K can be realized by radiative cooling. Therefore, vibration noise of cryogenic system is lower than that with heat links to cool the mirrors. It was reported that cooling of a mirror to 124 K without increasing the displacement noise was feasible [Shapiro 2017].

Silicon crystal can be grown up to the mass of around 400 kg with the diameter of 45 cm by current technology [Fisher 2012]. Mass of mirrors for Voyager and Cosmic Explorer is designed to be between 150 kg and 200 kg. The absorption at 1.5-2 um is quite low [C. Schinke 2015]. The absorption of a silicon, a resistivity of which was 10 kΩ·cm, was measured to be 4 ppm/cm [Degallaix 2013]. This value is much better than those of sapphire in KAGRA.

References:

- R. X. Adhikari *et al.*, Class. Quantum Grav. 37, 165003 (2020).
- R.X. Adhikari *et al.*, LIGO-T1400226-v10 (2024).
- D. F. McGuigan *et al.*, Journal of Low Temperature Physics 30, 621–629 (1978).
- K. G. Lyon *et al.*, Journal of Applied Physics 48, 865 (1977).
- B. Shapiro *et al.*, Cryogenics 81, 83–92 (2017).
- G. Fisher *et al.*, Proceedings of the IEEE 100, 1454-1474 (2012).
- C. Schinke *et al.*, AIP Advances 5, 067168 (2015).
- J. Degallaix *et al.*., Optics letters 38, 2047-2049 (2013).

3.2.5 Use of different materials for substrate

Version history: First version in 2024 by M. Eisenmann, S. Singh

Feasibility: 0 (no check performed at the required mass) In addition to sapphire and silicon discussed in previous sections, fused silica is the state of the art for test-masses substrates due to its high optical purity, large size availability along with well-developed polishing and coatings techniques. However, the mechanical quality of fused silica is quickly spoiled at cryogenic temperature and its low thermal conductivity makes it highly susceptible to thermal defects. The cryogenic temperature hence requires a crystalline material as test mass. As there is currently no demonstration of large ($> 40\ kg$) sapphire or silicon bulks at the required optical quality, it should be important to investigate the possibility of using other crystals as test-mass substrates. Some promising candidates are listed in Table 1. The ideal bulk material should exhibit (at least) properties such as, high thermal conductivity and low thermal expansion, low

absorption and birefringence, low loss angle, high density, availability in large size, and so on to be considered a favorable test mass candidate.

Material	Sapphire	MgF_2	Quartz	CaF_2	AlN	Diamond
Crystal Class	Trigonal	Tetragonal	Trigonal	Cubic	Hexagonal	Cubic
Transparency range [μm]	0.17-5.5	0.13-9	0.15-4.35	0.13-12	0.2-13.6	0.2-5
Absorption [ppm/cm]	90 @ 20K	-	-	20	< 100	300
Birefringence [Δn]	10^{-6}	0.012	0.011	0.228	0.2	$10^{-4} - 10^{-5}$
Expansion [$\parallel, \perp$] [$10^{-6}/K$]	5.6,5@293K	2.9,0.72@93K	7.97,13.37@273K	18.9@300K	2.6@300K	0.8
Conductivity [$\parallel, \perp$][W/m/K]	4.3×10^3@20K	21,33.6@300K	11.7,6.5@293K	39@83K	320@300K	1800-2200@300K
Optic coeff (n_o, n_e) [$10^{-6}/^\circ C$]	$\leq 9 \times 10^{-8}$@20K	1.1, 0.58	-	-10.5@297.15K	-	4.04-6.07
Q factor [10^8]	1	-	3.25@4K	-	-	-
Young's modulus [GPa]	344.5	138.5	97	75.79	273-346	1143
density [g/cm^3]	3.98	3.18	2.65	3.18	3.26	3.515
Size [radius,thickness][cm]	11.5, 15	10.16,10	-	10,10 (NBK)	5,0.1	-

Table 1: Properties at 1064 nm

References:

- Sapphire [Tomaru *et al.*2002]
- Quartz [Galliou *et al.*2011]
- MgF2 [2021]
- Handbook of Infrared optical materials, P klocek
- Temperature-dependent refractive index of CaF2 and Infralsil301, Douglas B. Leviton, Bradley J. Frey, Timothy J. Madison
- Lightmachinery CaF2
- new light photonics MgF2
- mse supplies MgF2
- crystran MgF2
- Diamond J M Dodson *et al.*
- Diamond Michael E. Thomas *et al.*
- Diamond Richard P. Mildren
- Quartz crystal IS, AlN substrate

3.2.6 Composite mass

Version history: First version in 2024 by K.Somiya
Feasibility: 0

Forming a mirror from multiple bulk instead of a single substrate is one way to increase the mass. The central part is a standard mirror and it is surrounded by additional substrates. DeSalvo performed finite element analysis to show that there exist nodes in the composite mass with no action band; i.e. no excess thermal noise from glue used to attache the additional parts [DeSalvo 2005].

Additional parts can be glued on the back surface of a mirror. While adding parts on side effectively increase the aspect ratio and possibly increase thermal noise, adding parts on the back surface does not increase the ratio. On the other hand, the additional parts on the back surface needs to have a sufficiently large aperture to transmit the beam.

An idea of the composite mass has been discussed time to time but there is no experimental demonstration.

References:

- R.DeSalvo, LIGO-050521 (2005)

3.2.7 Parametric instability mitigation

Version history: First version in 2024 September 21 by Kazuhiro Yamamoto. Second version in 2024 October 3 by Kazuhiro Yamamoto.
Feasibility: 5 (Mitigation methods (actuator and damper) are used in LIGO. However, the investigation for KAGRA is still necessary.)

Outlines of parametric instability

The parametric instability is caused by interaction between optical modes in Fabry-Perot cavities and elastic modes of mirrors. The thermal elastic vibration of the mirror converts a part of the Gaussian mode of cavity into higher optical modes. These higher optical modes apply the radiation pressure on the mirror surface. When the frequencies and shapes of the optical and elastic modes are similar, they excite each other effectively. The cavity keeps the high power higher optical modes and the mirrors vibrate largely. This is the parametric instability.

History of parametric instability investigation in KAGRA

The first investigation of the parametric instability of KAGRA (ICRR) was published in 2008 [K Yamamoto *et al.* 2008]. The most important conclusion is that the number of the unstable modes of KAGRA (only a few modes) is one order magnitude smaller than those of LIGO and Virgo. This number is proportional to the product of the mode densities of optical and elastic modes. Since KAGRA can adopt smaller beam radius (LIGO and Virgo must adopt larger beam to reduce mirror thermal noise), the KAGRA optical mode density is smaller. The sound velocity in sapphire (KAGRA) is larger than that in fused silica (LIGO and Virgo). This implies that KAGRA elastic mode density is lower. They are the reason why KAGRA unstable mode number is smaller.

KAGRA parametric instability was restarted (University of Toyama) after 2019. The details of KAGRA mirror shape (diameter, thickness, ears) were decided after the first KAGRA parametric instability investigation[K Yamamoto *et al.* 2008]. The KAGRA parametric instability was evaluated based on the specification details of sapphire mirrors installed in KAGRA interferometer. Only one unstable mode (84.7 kHz) was found [K Kaihotsu,2021]. This simulated mode frequency and shape are being checked experimentally [K Kaihotsu,2021][M Yamamoto,2024].

The simulation of the parametric instability has been started in NAOJ. The clipping effect of higher modes is being investigated.

Mitigation methods for KAGRA

Although the simulation and experimental check of simulation are done or in progress, mitigation investigation was not done. The mitigation strategies are summarized in [K Yamamoto *et al.* 2008]. The promising methods for KAGRA are feedback control and Q reduction of elastic modes. Since the KAGRA has only a few unstable mode, KAGRA might adopt only one of them.

For the feedback control, we have to check whether the coil magnet actuators or the photon calibrator [T Harder *et al.* 2023] for the sapphire mirrors can apply enough force to suppress the instability. LIGO successfully suppressed the parametric instability with the electrostatic actuator [C Blair *et al.* 2017]. At that time, the power in the main cavity is 100 kW and the actuator applied the force around 0.03 nN. The coil magnet actuator (maximum force at low frequency is on the order of 1 mN) can apply such small force. The design of the control servo is also necessary.

Reference [K Yamamoto *et al.* 2008] suggests the coating with mechanical loss on the mirror barrel surface as Q reduction method. When Q-values are on the order of 10^6, the instability is suppressed and thermal noise by this coating is enough small. The more realistic idea is the mechanical oscillator on the mirror barrel surface as like LIGO [S Gras *et al.* 2015] [S. Biscans *et al.* 2019] . The LIGO mushroom consists of the piezo, mass, and resistor. When the mirror elastic vibration is excited, the mass moves and the piezo between the mirror and mass stretches and shrinks. The voltage difference between both ends of piezo appears. The resistor, which is parallel to the piezo, has the current. This is the loss. Fortunately, the cryogenic stages with piezo are in the market (for example, [SmarAct])although the piezo efficiency has temperature coefficient [Physik Instrumente]. The appropriate resistor at cryogenic temperature is chosen. Even if the mechanical loss is not introduced intentionally, the bonding of sapphire suspension (or something else) could reduce Q-values. If this idea is correct, we need not to add any mechanical loss intentionally. We measured Q-values of the sapphire mirrors at the site and derive the loss distribution from the measured Q-values and finite element simulation. Then we evaluate parametric instability and the thermal noise. In any cases, how much the loss in the mirrors reduce elastic Q and contribute thermal noise must be investigated.

Recently new mitigation schemes are investigated, optical feedback. The higher optical mode with opposite phase is injected [V Bossilkov *et al.* 2014].

Phase camera is used to monitor mirror vibration (reference must be looked for).

Recycling effect

The simulation with recycling must be considered. The recycling effect in KAGRA was not investigated well. The KAGRA recycling scheme can be changed. The latest update of recycling scheme must be the reference.

References:

- K Yamamoto, T Uchiyama, S Miyoki, M Ohashi, K Kuroda and K Numata J. Phys.: Conf. Ser. 122, 012015 (2008).
- K Kaihotsu Master thesis (Japanese), University of Toyama (2021).
- M Yamamoto Master thesis (Japanese), University of Toyama (2024).
- Thomas Harder, Margherita Turconi, Rémi Soulard, and Walid Chaibi Optical Express 31, 1486 (2023).
- C Blair and LSC Instrument Authors Phys. Rev. Lett. 118, 151102 (2017).
- S. Gras, P. Fritschel, L. Barsotti, and M. Evans Phys. Rev. D 92, 082001 (2015).
- S. Biscans, S. Gras, C.D. Blair, J. Driggers, M. Evans, P. Fritschel, T. Hardwick, and G. Mansell Phys. Rev. D 100, 122003 (2019).
- Web site of SmartAct Web site of SmartAct.
- Web site of Physik Instrumente Web site of Physik Instrumente.
- Vladimir Bossilkov, Jian Liu, Carl Blair, Chunnong Zhao, and Li Ju Phys. Rev. D 109, 102006 (2024).

3.2.8 Thermal compensation system

Version history: First version in 2019 white paper; updated by Haoyu in September in 2024.

Feasibility: 5 (Demonstrated by LIGO and Virgo)

Thermal compensation system is one of the techniques well developed in LIGO and Virgo but not in KAGRA. The current method cannot be applied to the KAGRA test masses with high thermal conductivity. It can be applied as is, however, for the beam splitter and the power recycling mirrors.

One possible usage of the thermal compensation system in KAGRA is to compensate the thermal lens in the beam splitter, through which ca 250 W laser beam can transmit. A discussion about the necessity of the compensation system for KAGRA BS was made in early days to conclude it is not too much necessary, but it would be more and more needed if we increase the circulating power.

Another usage is for fine mode-matching of the power- and signal-recycling cavities. The PR2/3 or SR2/3 mirrors were to play a role of the fine mode matching but in reality it is not easy to move those mirrors suspended under the heavy Type-Bp or Type-B system. The thermal compensation system can achieve this more easily and would be necessary in the near future. But note that this is fine mode-matching with thermally tuning, not thermal compensation.

3.2.9 Use of different materials for coatings

Version history: First version in September 2024 by S. Tanioka and M. Eisenmann

Feasibility: 2 (Various research are ongoing)

The design sensitivity of KAGRA is partially limited by coating thermal noise (CTN) arising from amorphous silica and tantala (SiO_2/Ta_2O_5) coatings. Recent study on cryogenic coating mechanical loss showed SiO_2/Ta_2O_5 coatings can have higher mechanical loss than the designed value, resulting in worse sensitivity [Mori *et al.* 2024]. In order to enhance the GW detection rate, and hence their scientific impact, lower thermal noise mirror coatings need to be developed. The next upgrade to the LIGO detectors, called Advanced LIGO+, is aiming a reduction of CTN by about a factor of 2 compared to that of current Advanced LIGO detector. Titania doped germania ($Ti : GeO_2$) and titania doped silica ($Ti : SiO_2$) are possible candidates for that [Vajente *et al.* 2021, McGhee *et al.* 2023]. $Ti : GeO_2$, however, is still suffering from blistering and crystallization after thermal treatment as well as larger optical absorption compared to that of current coatings. $800\,C^\circ$ heat treated $Ti : SiO_2$ has shown promising CTN and optical absorption at room temperature though its Raman spectrum indicates the possibility of crystallization, which is generally considered undesirable for high-end mirrors. Further investigations are still needed to implement these coatings in a gravitational wave detector.

Other amorphous coatings are also extensively being studied. Amorphous silicon (aSi) is a possible candidate to improve the sensitivity thanks to its low mechanical loss at cryogenic temperature. However, it has a large optical absorption which can degrade the performance of the detector [Birney *et al.* 2018]. One possible solution to mitigate the large absorption in aSi is to employ multimaterial coatings [Steinlechner *et al.* 2021]. In addition to aSi coatings, wide range of amorphous coatings are being studied, for instance fluoride based coatings and amorphous silicon carbide (a-SiC) [Granata*et al.* 2022, Favaro *et al.* 2022] However, none of them have shown promising results for applications to GWDs. Employing optimized coating layers or nanolayered coatings are also possible approaches to reduce CTN, but of course further research is needed [Cuo *et al.* 2019, Venugopalan *et al.* 2024].

Crystalline AlGaAs coatings are a possible coating candidate for future upgrade of Advanced LIGO because of its low mechanical loss [Cole *et al.* 2023]. While crystalline AlGaAs coatings can largely reduce the CTN, recent studies with cryogenic silicon cavities have observed unknown noise sources; birefringent noise and global noise [Kedar *et al.* 2023, Yu *et al.* 2023]. Further investigations

are necessary to determine if this technology can be applied to detectors. In addition, current arm-length stabilization (ALS) system is not compatible with AlGaAs coatings due to the narrow band gap of GaAs; thus a new ALS scheme needs to be installed such as shown in [Tanioka *et al.* 2024].

Finally, we would like to mention the results of direct CTN measurements at cryogenic temperature by JILA and PTB [Robinson *et al.* 2021]. Their results indicate that the mechanical loss of SiO_2/Ta_2O_5 coatings around 20 K is about 3×10^{-4}, which can lead to a lower CTN level in KAGRA than the design value. Considering the excellent optical properties (especially optical absorption) of current SiO_2/Ta_2O_5 coatings, which is suited for cryogenic operation, developing an alternative coatings for KAGRA is not urgent for O5. R&Ds, however, are essential toward post-O5 upgrades as the CTN may limit the sensitivity by reducing other noise levels.

References:

- Y. Mori *et al.*, Physical Review D **109**, 102008 (2024)
- G. Vajente *et al.*, Physical Review Letters **127**, 071101 (2021)
- G. I. McGhee *et al.*, Physcial Review Letters **131**, 171401 (2023)
- R. Birney *et al.*, Physical Review Letters **121**, 191101 (2018)
- J. Steinlechner and W. Martin, Physical Review D **42**, 042001 (2021)
- M. Granata *et al.*, Physical Review Applied **17**, 034058 (2022)
- G. Favaro *et al.*, Physical Review Applied **18**, 044030 (2022)
- L-C. Cuo *et al.*, Optics Letters **44**, 247-250 (2019)
- G. Venugopalan *et al.*, Optics Express **32**, 11751-11762 (2024)
- G. D. Cole *et al.*, Applied Physics Letters **122**, 110502 (2023)
- D. Kedar *et al.*, Optica **10**, 464-470 (2023)
- J. Yu *et al.*, Physical Review X **13**, 041002 (2023)
- S. Tanioka *et al.*, Optics Letters **49**, 5763-5766 (2024)
- J. M. Robinson *et al.*, Optics Letters **46**, 592-595 (2021)

3.2.10 Non-TEM00 beam

Version history: First version in 2019 white paper; Edited by Haoyu in September in 2024.

Feasibility: 3 (A. Noack demonstrated with a table-top in 2017)

The coating thermal noise can be reduced by increasing the beam spot size, thus averaging better over the coating thermal noise component of the test masses. There has been investigation into increasing the area of the intensity

distribution of the beam by using alternative beam shapes. Possible candidates are conical beams [Bondarescu 2007], mesa beams [Bondarescu *et al.*2006] and higher-order Gaussian modes [Chelkowski *et al.*2009]. These beams have a wider intensity distribution than the current used fundamental mode (TEM00). Conical and mesa beams require more complex mirror profiles [Bondarescu *et al.*2008]. The Laguerre-Gauss 33 (LG33) mode [Fulda *et al.*2010] produced by standard spherical mirrors is a more promising alternative. It offers the best trade-off between thermal noise reduction and clipping losses in the current detector architecture. Therefore, it has been proposed for an upgrade of aLIGO and for the proposed [Einstein Telescope 2008].

Optical cavities are crucial elements of GW detectors in achieving the required interferometer sensitivity: they reduce beam pointing and power noise; the coupled cavities increase the power in the two arms of the interferometer to improve the detector sensitivity; and cavities act as mode cleaners to filter the spatial beam profile. Therefore, the higher-order mode technique has to be compatible with the cavities if it is to be implemented in these detectors. However, recent research drew attention to several problematic effects of higher-order LG modes in cavities: first, three-mirror cavities do not transmit helical LG modes due to their phase profiles. Second, due to mirror distortions of the arm cavity mirrors, the detector readout sensitivity is reduced, as the light of the LG33 mode is coupled to other modes of the ninth order. Third, the expected degeneracy of the modes of the same order broke in a 10 m high finesse linear cavity due to astigmatism so that a LG33 mode could not be resonantly enhanced. While mirrors with a smoother surface could reduce the latter two effects, three-mirror cavities must not be used in future detectors if the LG33 mode is used [Noack *et al.*2017].

References:

- M. Bondarescu, Doctoral dissertation, California Institute of Technology, 2007.
- M. Bondarescu *et al.*, Physical Review D **74**, 082003 (2006).
- S. Chelkowski *et al.*, Physical Review D **79**, 122002 (2009).
- M. Bondarescu *et al.*, Physical Review D **78**, 082002 (2008).
- P. Fulda *et al.*, Physical Review D **82**, 012002 (2010).
- P. Fulda, Doctoral dissertation, University of Birmingham, 2012.
- C. Bond *et al.*, Physical Review D **84**, 102002 (2011).
- A. Noack *et al.*, Optics Letters **42(4)**, 751-754 (2017).

3.2.11 Non-cylindrical mass

Version history: Briefly mentioned in the version in 2019; updated in 2024 by K.Somiya

Feasibility: 0

One of the reasons why a C-axis sapphire substrate cannot be large is because the crystal grows in the A-axis direction with the standard Czochralski method. A C-axis cylindrical mirror is made by curving the A-axis cylinder, wasting large fraction of bulk. One naive idea to increase the sapphire mass is to make use of the wasting parts [Somiya 2010]. The substrate would then look like a kamaboko, a Japanese fish cake. This *kamaboko mirror* was not favored, however, for a possible challenge of the surface polishing.

References:

- K.Somiya, "Alternative technologies?" presentation at the 3rd ET General Meeting, Budapest (2010)

3.2.12 Khalili cavity

Version history: First version in 2019 by K.Somiya

Feasibility: 1

Another way to reduce coating thermal noise would be to replace a test mass with many-layer coatings by a pair of mirrors with less layers, or by an unwedged substrate with both surfaces coated. This technique is known as a Khalili cavity [Khalili, 2005] or a Khalili etalon [Somiya 2011]. With the distance between the two surfaces kept anti- resonant for the laser beam, the reflectivity of the cavity or the etalon can be as high as a thick-coating mirror but coating thermal noise of the back surface is not probed as much as the front surface as most of the beam is reflected by the front surface.

References:

- F.Khalilia, Phys. Lett. A, 334, 67 (2005)
- K.Somiya, *et al.*, Phys. Lett. A, 375, 1363 (2011)

3.2.13 Gratings

Version history: First version in October 2024 by S. Tanioka

Feasibility: 2 (Demonstration with a silicon cavity is on going by a German group)

A coatingfree mirror can remove coating thermal noise in principle. One possible approach to realize a coatingfree mirror is to apply a nanostructured surface on a substrate to form a waveguide grating mirror [C. F. R. Mateus *et al.* 2004]. By optimizing the substrate material and its grating structure, the thermal noise level can be largely suppressed [J. Dickmann *et al.* 2018].

Extensive research has been conducted in order to realize high-reflective waveguide grating mirrors. In 2010, a power reflectivity, R, of 99.8% at 1550 nm wavelength was achieved with monocrystalline silicon [F. Brückner *et al.* 2010]. In 2023, $R = 99.95\%$ mirror was demonstrated by combining with a etalon [J. Dickmann *et al.* 2023]. Further R&Ds, however, are needed to achieve $R >$ 99.99%, which is required for end test masses in gravitational wave detectors. In

addition, there is a technical challenge to achieve low optical losses since grating mirrors often suffer from higher scattering losses. Scaling up the size is also an issue that needs to be addressed.

On the other hand, gratings might be useful for recycling mirrors instead of test masses. As shown in [J. Dickmann *et al.* 2023], the reflectivity is variable depending on the polarization of the incident beam. If this technology is employed for the signal recycling mirror (SRM), one can tune the reflectivity of the SRM without replacing mirrors. This will provide flexibility in interferometer design.

References:

- C. F. R. Mateus *et al.* IEEE Photonics Technology Letters **16**, 518-520 (2004)
- J. Dickmann *et al.* Physics Letters A **382**, 2275-2281 (2018)
- F. Brückner *et al.* Physical Review Letters **104**, 163903 (2010)
- J. Dickmann *et al.* Commun. Phys. **6**, 16 (2023)

3.3 Cryogenic cooling

3.3.1 Radiative cooling

3.3.2 Reducing vibration of cryogenic components

Version history: First version in 2024 by Rishabh Bajpai
Feasibility: 3/4 (Cancellation of cryocooler vibration by out of phase operation of cryocoolers has been demonstrated by CUORE. Also, cryocoolers including active vibration isolation setups have been developed.)

Mechanical cryocoolers provide a safe and relatively cheap way to cool down components to cryogenic temperatures. However, the mechanical vibration from the cryocooler is a potential noise source and could contaminate the detector's sensitivity. In the case of KAGRA, this vibration couples to the mirror through the thin Al-heatlink, which are used for conduction cooling.

The vibration analysis of one of the KAGRA cryostats (IYC) was conducted at cryogenic temperature. It was found that the vibration of the radiation shield is 2–3 orders of magnitude larger than Kamioka seismic motion in the 1–100 Hz band due to the internal resonance of the cooling system and operation of the cryocooler. The operation of cryocoolers does not change the noise floor (anyhow larger than the seismic noise), but 2 Hz peaks and their harmonics were observed. The impact of this vibration on KAGRA sensitivity was also evaluated and it is below the design requirement. The details of this measurement can be found in [Bajpai *et al.*2022].

While this vibration is not an issue with the current design sensitivity, it may become problematic in the future when we try to push past the design sensitivity. Furthermore, by reducing this vibration, we might be able to increase the number of heat links between the cooling bar and cryogenic payload, increasing the thermal conducitivity.

Two possible approaches to reducing the cryocooler vibration have been practically demonstrated (not directly in GWDs). One approach is to introduce some active actuation to cancel the vibration. This is employed in the Vibration Free Cryostat of ROMA University. Furthermore, the LiteBIRD group in QUP, KEK, is developing a similar cryocooler. (*need citation*) Another approach can be to cancel out the vibration of a pair of cryocoolers by operating them out of phase. This approach has been used in CUORE (neutrino-less double beta decay experiment) as shown in [D'Addabbo *et al.*2018]. However, phase optimisation is necessary for CUORE since the coldhead distribution is asymmetric. In the case of KAGRA, this approach could be much more straightforward due to the symmetric positioning of the cold head (opposing cryocoolers can be operated out of phase). One issue is that cooling efficiency may fall and take longer to cool down. However, this out-phase operation can only be used during the observation phase. The test of this approach using one of the KAGRA cryostats was proposed by Ettore Majorana [Majorana *et al.*2019]. However, a practical experiment was never conducted. This relatively simple demonstration can be conducted at the KAGRA site within a few months.

References:

- Bajpai *et al.,* Classical Quantum Gravity 39, 165004 (2022).
- D'Addabbo *et al.*, Cryogenics 93 (2018) 56-65
- Majorana *et al.*, Presentation at F2F Dec. 2019

3.4 Cryogenic suspensions

3.4.1 Sapphire blade spring improvement

Version history: First version in 2024 by Rishabh Bajpai

Feasibility: 2 (Active RD experiments going on in ET on sapphire and silicon)

Since sapphire has high stiffness, the stretch of the fibres is a few tens of μm when suspending the 23 kg sapphire mirror. This stretch is smaller than the length fabrication error of the fiber. Blade springs are M-shaped sapphire parts that compensate for the difference in fiber length. The blades are clamped to the IM with copper clamps, and the fiber nail head is glued to the blade spring using gallium.

The Q requirement to reach KAGRA design sensitivity is 1.4×10^6. However, the highest measured Q by Yamada *et al.* was 1.3×10^5 (for the first mode). This Q is limited by the losses at copper clamping and not the blade spring itself. Eventually, the blade spring Q should be limited by the complex shape of the blade springs (high-stress unpolished regions), but the first step should be improving the clamping. ROMA University is testing a new blade spring design [Majorana *et al.*2023].

Given the high cost of procuring prototypes and the lack of volunteers available for Q measurement experiments, enhancing collaboration with ET will be vital to improving the blade spring and the entire sapphire suspension.

References:

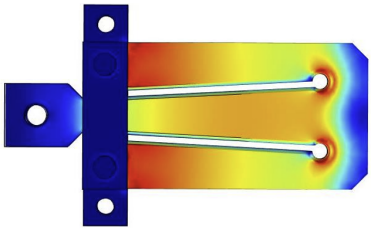

Figure 4: Simulation of stress distribution in blade spring bending mode.

- Yamada *et al.*, Presentation at GWREM 2019.
- Majorana *et al.*, *Cryogenic Payload Prototype at ARC*Poster Presentation at GWADW 2023.

3.4.2 Use of ribbons

Version history: First version by KK in Oct. 1st, 2024.Additional info by Bajpai
Feasibility: 1 or 3 (Many theoretical studies have been conducted since 20th century but probably no experimental demonstration so far)

Suspension thermal noise is one of fundamental noises in the gravitational-wave detectors regardless of operation under room or cryogenic temperature. In the power spectrum density, it typically appears as a broadband noise between 10-100 Hz and as peak-shaped noises called violin modes above 100 Hz. Suspensions with rectangle profiles, i.e., ribbon-shaped fiber, in contrast to conventional cylindrical one, have been studied to further reduce the broadband suspension thermal noise and negative effects of the violin modes.

The concept of the ribbon suspension was discussed in the context of targetting at high-Q pendulum by membrane suspension while increasing the violin frequencies out of the detector band [Blair *et al.*1993]. Although the target was aLIGO at room temperature, trade-off of the cylindrical fiber and ribbon has been studied with taking the suspension thermo-elastic noise into account [Gretarsson *et al.*2000]. Orthogonal ribbons had been proposed to reduce the number of violin modes to less than half with maintaining the broadband noise at low frequencies [Lee *et al.*2005]. A potential upgrade of aLIGO named as Voyager operated in cryogenic temperatures will adopt the ribbon suspension made of Silicon [Adhikari *et al.*2020]. In the context of KAGRA, a study of non-uniform fiber, in particular, flexure plus strut fiber, has been performed [Sekiguchi *et al.*2012].

Many theoretical studies have been conducted so far, however, there is little experimental demonstration. It is because the advantages of the ribbon suspension cannot surpass a technical risk of manufacturing and implementation on the actual gravitational-wave detectors. ARC Group, ROMA University is working

with Kyocera (Japan) to develop an ET-size monolithic sapphire fiber (ribbon+ear). The expected delivery date is six months (as of 17/10/2024). *(need citation? personal communication with E. Majorana and visit to Kyocera)*
References:

- D. G. Blair *et al.*, Rev. Sci. Instrum. 64, 1899 (1993).
- A. M. Gretarsson *et al.*, Phys. Lett. A 270, 108 (2000).
- B. H. Lee *et al.*, Phys. Lett. A 339, 217 (2005).
- R. X Adhikari *et al.*, Class. Quantum Grav. 37, 165003 (2020).
- T. Sekiguchi *et al.*, JGW-G1200859 (2012).

3.4.3 Use of long fibers

Version history: First version by KK in Oct. 2nd, 2024.
Feasibility: 1 (Theoretically well studied but no experimental demonstration in 2024)

The dilution factor of the fiber mechanical loss is proportional to the fiber length, and the power spectrum density of the suspension thermal noise is inversely proportional to square of the fiber length. Therefore, as well as decreasing the fiber thickness, increasing the fiber length also leads to effective reduction of the suspension thermal noise.

Employment of long fibers is mainly considered in the upgrade plan of current detectors. Among various candidates of upgraded aLIGO, LIGO Low Frequency (LF), which focuses on improved sensitivities in 5-30 Hz, will double the length of the suspension for test masses to 1.2 m [Yu *et al.*2018]. KAGRA's upgrade plans also include the low-frequency option expanding the suspension from 35 cm to 1 m [Michimura *et al.*2020], constrained by the current inner shield height in the cryostat, which is approximately 1.6 m. ET-LF [Koroveshi *et al.*2023] and CE [Reitze *et al.*2019] will also utilize the long fiber of 2 m and 1.2 m, respectively.

The long fiber has a disadvantage of low violin frequencies contaminating typical GW frequency band around 100 Hz. However, this will not be a critical problem because the low-frequency upgrading plan will target at frequencies below 100 Hz. To our knowledge, there is no experimental demonstration of the meter-scale suspension.

Reducing the suspension thermal noise by thinning the fiber, rather than extending its length, is a potential alternative. This approach has the advantage of avoiding adjustments to the suspension balance or vibration isolation, which may be affected by changes in suspension length. While the dilution factor depends similarly on fiber length and diameter, a thinner fiber has reduced cooling capacity; because energy absorption scales with fiber length and the square of its diameter, thinning the fiber raises mirror temperature more than lengthening it by the same factor.
References:

- H. Yu *et al.*, Phys. Rev. Lett. 120, 141102 (2018).
- Y. Michimura *et al.*, Phys. Rev. D 102, 022008 (2020).
- X. Koroveshi *et al.*, Phys. Rev. D 108, 123009 (2023).
- D. Reitze *et al.*, Bull. Am. Astron. Soc. 51, 035 (2019).

3.4.4 High conductivity fibers

3.5 Other optics

3.5.1 Large beamsplitter

Version history: First version in 2024 by H. Wang.
Feasibility: 5

Thermo-refractive noise is the most dominating noise source of the beam splitter [Benthem 2009] due to the very low mechanical loss of fused silica at room temperature and the small number of coating layers. Due to the fact that this element is situated outside the arm cavities its thermal noise contribution to the overall thermal noise of the detector small. Since the beam splitter is operated under an angle, the necessary size is increased (compared to an end mirror) to avoid the clipping loss. If larger beam spot size on cavity mirrors is used, the size of the beam splitter should be also increased. The larger laser beam at the beam splitter is beneficial for reducing thermo-refractive noise. The necessity of using larger beam splitter really depends on the level of thermo-refractive noise and if larger beam size is used.

Table 2 shows the BS size and beam size in KAGRA, Advanced LIGO and Advanced Virgo. Advanced LIGO plans to replace its current BS with larger size due to the large clipping loss for squeezing.

Table 2: Comparison of the BS size and beam size in different detectors. Numbers in the bracket are from the design of the new BS for Advanced LIGO.

	KAGRA	aLIGO	Advanced Virgo
BS diameter (mm)	370	370 (450)	550
BS thickness (mm)	80	60 (60 or 73)	65
Beam radius (mm)	36	53	49
Beam diameter on BS (mm) (45 deg. incidence)	102	150	139
BS and beam size ratio	3.6	2.5 (3.0)	4.0

References:

- B. Benthem *et al.*, Physical Review D **80**, 062004 (2009).

3.5.2 Low-loss Faraday isolator

Version history: First version in 2024 by K.Somiya
Feasibility: 5

While the KAGRA IFI was developed by the team in Univ of Florida, who also developed the aLIGO IFI and A+ OFI, and then assembled and installed by the joint team of UFL and Tokyo Tech, the 1st phase KAGRA OFI was developed by the team in Tokyo Tech using commercially available optics. The requirement for the 1st phase OFI was set to 90 percent transmission and 25dB isolation. The requirement for the 2nd phase OFI was 97 percent transmission and 35dB isolation.

The KAGRA OFI is composed by two quartz rotators purchased from ATF, two Blewster angle PBS purchased from ATF, and one ϕ 12 mm Faraday rotator (TGG) purchased from EOT. The measured transmission and isolation were 95 percent and 28dB, respectively [Otabe 2018].

The A+ OFI is composed by one fused silica prism for an angle compensation, one KTP prism, one quartz rotator, one thin film polarizer, and one ϕ 20 mm TFF. The measured transmission and isolation were 99.55 percent and 38.5dB, respectively [Martin, 2021].

A large KG5 glass with an aperture is placed at the input of the KAGRA OFI. It is inclined vertically in 56 deg so that the S polarization junk light can be dumped. Since we did not recognize the birefringence of ITM at the time of the OFI installation, the P polarization junk light is not taken care; nearly 10 percent of it will be reflected by the large KG5 toward the ceiling of the OMC chamber.

KG5 glasses are placed at most locations to dump the reflected beams. Beams are dumped twice, once at the Brewster angle for the P polarization light and then again at the normal incidence.

The OFI breadboard equips holes at the corners to be suspended, but it is currently not suspended. Our estimation in 2018 did not require a seismic isolation of OFI. With a larger amount of scattering due to the ITM birefringence, the OFI should better be suspended.

References:

- S.Otabe, JGW-G1808214-v14 (2018)
- R.Martin, presentation at GWADW, LIGO-G2101056 (2021)

3.5.3 Low-loss OMC

Version history: First version in 2024 by K.Somiya
Feasibility: 5

The phase-1 KAGRA OMC was developed and installed by the Tokyo Tech team with help of Caltech (for optical and electronical design) and UWA (for suspension design). The optical system was designed with a thorough modal model simulations using fake mirror maps with reasonable PSD; mirrors were

not available at the time. Suspension tests and Gouy phase measurements were performed in success at Tokyo Tech before the shipping to KAGRA.

Later, a misalignment of the first OMC mirror was found, and the NAOJ team fixed it. The transmission measured after the refurbishment was 58 percent, and it turned out the first OMC mirror had become somehow contaminated. The NAOJ team replaced the mirrors and the transmission improved but to 85 percent. This is still much lower than that in aLIGO which is 97 percent.

The phase-1 OMC has a number of issues. Some were known before the installation and some were found later. One known issue is the thermal expansion of the OMC breadboard that is made of aluminium. The piezo actuator has a larger dynamic range than LIGO's to compensate the large thermal expansion. The OMC can be kept on resonance if the temperature change in the chamber is less than one point. Another known issue is the heat emission from the PD. The original design was to coat the PD mounts by alumina, but the plan was rejected by the VAC subsystem due to the lack of evidence. Instead, we attached an alumina plate with indium foil inserted to emit the heat from the aluminium PD mount and the aluminium breadboard. In the end, some fraction of heat is emitted from the plate on the mount and some other fraction of heat goes through the PEEK base to the breadboard and then emitted from the big plate. The latter fraction of heat increases the temperature of the breadboard.

One of the issues we found after the installation was a poor isolation ratio of the OMC table. We used a measured data in TAMA but it turned out the stack rubber was different from the one in TAMA and the isolation ratio does not seem to be as good. Another issue is the excitation of the OMC breadboard in a bending mode. The vertical motion of the suspended breadboard couples to the bending mode and changes the OMC length. An improvement is on-going.
References:

-

3.5.4 Low-loss PD

Version history: First version in 2019 by M. Leonardi; summarized in October 2024 by Y. Michimura
Feasibility: 3 (Photon recycling demonstrated by K. Nagano in 2018)

Improving the quantum efficiency of the photodiodes that detect gravitational wave signals is a straightforward way to improve the performance of KAGRA. An this moment, according to the KAGRA sensitivity simulation code, the photodiode quantum efficiency is set at 0.9. This includes various optical losses in the detection chain. For both BRSE and DRSE configuration, improvement of about 0.4dB at high frequency can be possible by using a higher efficiency of 0.99).

LIGO currently uses photodiodes with a efficiency of 0.98 [Tse 2019]. Further improvement would be possible using photon recycling technique [Nagano 2018]. Photodiodes with high quantum efficiency at different wavelengths would also be necessary for different wavelengths (see Sec. 3.1.2).

References:

- M. Tse *et al.*, Phys. Rev. Lett. 123, 231107 (2019).
- K. Nagano *et al.*, Applied Optics 57, 3372 (2018).

3.6 Low frequency noise reduction systems

3.6.1 Adaptive control for better seismic isolation

Version history: First version in October 2024 by M. Tamaki
Feasibility: 4 (demonstrated with a 40 m protptype at Caltech)

Seismic motion is one of the fundamental noise sources in low-frequency band and must be minimised in order to detect the tiny displacements of the mirrors caused by gravitational waves. At KAGRA, the effect of seismic motion through the main interferometer mirrors is mitigated by suspensions (Type A, B, Bp suspensions) tailored to specific requirements. In particular, the Type-A and B suspensions include pre-isolators consisting of inverted pendulums and GAS filters, which provide active vibration isolation below 1 Hz using sensors such as linear variable differential transducers and geophones. To achieve better seismic isolation, active control needs to be optimised. For example, sensor fusion, which uses $\mathcal{H}_\infty$ synthesis to identify the sensor combination with the lowest noise at each frequency, and sensor correction, which converts the relative position between the platform and reference platform into inertial readout, have been implemented in the pre-isolator control of the Type-B suspensions [Tsang *et al.*2024]. Implementing these methods to the Type-A suspensions is a potential improvement.

However, it is important to note that seismic noise are not static; they vary due to factors such as earthquakes and weather conditions, and there are even seasonal changes. Therefore, a static control filter designed for a specific date and time may not always be optimal. To address this, control strategies such as adaptive control can be considered. This approach continuously updates control parameters in real time, ensuring optimal performance even when the noise affecting the system is dynamic [Zuo *et al.*2005]. In seismic isolation, for example, real-time measurements of seismic noise can be used to optimise loop gain: the gain can be increased during periods of large seismic motion and reduced when activity is lower to minimize noise intrusion. Adaptive control has been tested in the 40 m prototype interferometer lab at Caltech [Driggers *et al.*2012].

In implementing this control, how the cost function is chosen (e.g., RMS motion) is very important and should be considered carefully. However, if adaptive control is designed well, it will reduce seismic noise-derived lock losses and will contribute to improving duty cycle.

References:

- T. Tsang *et al.*, arXiv:2407.15972 (2024)

- L. Zuo *et al.*, IEEE Transactions on Control Systems Technology, **13** 4 (2005)
- J. C. Driggers *et al.*, Review of Scientific Instruments, **83** 024501 (2012)

3.6.2 Better damping control

Version history: First version in October 2024 by M. Tamaki
Feasibility: 5 for global damping / 3 for local sensor development

As for payload part, the pendulum system to mitigate seismic noise exhibits resonances with exceptionally high quality factors. Active damping of these resonant modes is essential, yet sensor noise from this control can significantly impair the interferometer's sensitivity within the observation band. At KAGRA, local damping control noise from the suspension system is a prominent source of noise in the 10 to 100 Hz range, occasionally limiting sensitivity.

One approach to mitigating this noise is the implementation of global damping, as demonstrated in advanced LIGO [Shapiro *et al.*2015]. This method performs a coordinate transformation from the local reference frame to the one aligned with the interferometer readout, allowing the use of less noisy interferometer signals for damping control. Global damping can isolate the effects of local sensor noise, allowing more aggressive damping and the construction of a more robust cavity. Another major advantage of global damping is that it allows damping control and interferometer control to be performed independently, reducing the likelihood that changes in one control system will affect the other.

Another approach focuses on enhancing local sensors. Currently, KAGRA employs reflective photosensors (for Type-A suspensions) and shadow sensors known as OSEMs (for Type-B and Bp suspensions) for payload damping. However, interferometric sensors generally offer superior precision and lower noise compared to electromagnetic-based sensors like photosensors or OSEMs. In fact, the development of lower noise sensors has been active in recent years. For instance, Homodyne Quadrature Interferometers (HoQIs) exhibit noise levels approximately three orders of magnitude lower than the improved OSEMs (BOSEMs) [Mitchell *et al.*2024]. Studies have shown that using these advanced sensors for suspension control can significantly improve damping performance [Dongen *et al.*2023]. While technical challenges—such as cryogenic operation for KAGRA's main sapphire mirrors—may arise, developing interferometric sensors would be highly beneficial in reducing damping control noise.
References:

- B. N. Shapiro *et al.*, Class. Quantum Grav. **32**, 015004 (2015)
- A. Mitchell *et al.*, arXiv:2409.08843 (2024)
- J. van Dongen *et al.*, Rev. Sci. Instrum., **94**, 054501 (2023)

3.6.3 Low-frequency vibration isolation

Version history: First version in 2024 by Kohei Mitsuhashi

Feasibility: 3 (K.Mitsuhashi demonstrated with a table-top in 2023)

The sensitivity of the low-frequency band in laser interferometer gravitational wave detector is fundamentally limited by seismic noise. In current detectors such as aLIGO, AdVirgo, and KAGRA, mechanical low-pass filters, using pendulums and springs, serve as vibration isolation systems to protect the detectors from seismic noise. Therefore, to improve the sensitivity in the low-frequency band beyond current detectors, as aimed for in the Einstein Telescope (ET), one of the third-generation gravitational wave detectors, it is essential to adopt more high-performance vibration isolation systems than the existing ones. As a response to this requirement, ET plans to implement a two-stage low-frequency vibration isolation system[ETpathfider Team 2020], using inverted pendulums (IP)[A. Takamori *et al.* 2007], which are already employed in KAGRA. This low-frequency vibration isolation system achieves a compact structure and a low resonance frequency (below 1 Hz) by utilizing the design of pendulums or physical properties.

In addition to IP, there are several designs for low-frequency vibration isolation systems, one of which is the Roberts' Linkage (RL). The resonance frequency of RL is determined by the relationship between the suspended points and its center of mass. In the 2000s, a four-point suspended RL was researched and developed at The University of Western Australia[F. Garoi *et al.* 2003][Pablo Barriga *et al.* 2009]. In NAOJ, we conducted theoretical[M.Otuka *et al.*] and experimental research on a three-point suspended RL, which eliminates the possibility of performance degradation caused by differences in tension on the suspension wires. In experiments, it was confirmed that raising the center of mass lowers the resonance frequency, which aligns with theoretical predictions. The lowest measured resonance frequency was 34 mHz. Furthermore, it was experimentally verified that the resonance frequency drifts when the horizontal position of the center of mass is altered.

Additionally, we made a two-stage low-frequency vibration isolation system by adjusting the resonance frequencies of both the IP and the three-point suspended RL to approximately 70 mHz and measured its transfer function. The results showed that double-stage isolation was achieved from below 100 mHz.

References:

- ETpathfinder Team, The ETpathfinder DESIGN REPORT. (January 2020).
- A. Takamori *et al.*, Inverted pendulum as low-frequency pre-isolation for advanced gravitational wave detectors, Nuclear Instruments and Methods in Physics Research Section A: Accelerators, Spectrometers, Detectors and Associated Equipment, Volume 582, Issue 2 (2007).
- F. Garoi *et al.*, Passive vibration isolation using a Roberts linkage, Review of Scientific Instruments, Vol. 74, No. 7, pp. 3487–3491, (2003).
- Pablo Barriga *et al.*, Compact vibration isolation and suspension for australian international gravitational observatory: Performance in a 72 mfabry perot cavity, The Review of scientific instruments, Vol. 80, p. 114501, (2009).

- M. Otsuka *et al.*, Theoretical Characteristics of a Three-Point Suspended Roberts Linkage, in private communication.

3.6.4 Suspension point interferometer

Version history: First version in 2019 by S. Haino; Summarized in November 2024 by Y. Michimura and M. Ando
Feasibility: 3 (Y. Aso demonstrated with a table-top in 2004)

Suspension Point Interferometer (SPI) was once considered as one of the options for reducing vibrations introduced from heat-links and for robust lock acquisition for LCGT [JGW-T0900056]. In the SPI concept, Fabry-Perot interferometers are formed using upper stage masses of main test mass suspensions of arm cavities. By locking the SPI, the main arm cavity length fluctuations from external vibrations are reduced.

A prototype Fabry–Perot interferometer equipped with an SPI was constructed and vibration isolation in both the spectrum and transfer function were observed. The noise spectrum of the main interferometer was reduced by 40 dB below 1 Hz. Transfer function measurements showed that the SPI also produced good vibration suppression above 1 Hz. These results indicate that SPI can improve both the sensitivity and the stability of the interferometer [Physics Letters A 327, 1 (2004)].

The SPI working group recommended not to install SPI to LCGT mainly because it is over-kill compared with the minimum technology to achieve the design sensitivity. More detailed reasons are summarized in the report [JGW-T0900056].
References:

- LCGT SPI Special Working Group, *Study report on the LCGT Suspension Point Interferometer*, JGW-T0900056 (2009).
- Y. Aso, M. Ando, K. Kawabe, S. Otsuka, K. Tsubono, Physics Letters A 327, 1 (2004).
- Y. Aso, *Active Vibration Isolation for a Laser Interferometric Gravitational Wave Detector using a Suspension Point Interferometer*, Ph.D Thesis, The University of Tokyo (January, 2006).

3.6.5 Vertical suspension point interferometer

Version history: First version in 2019 by S. Haino; Summarized in November 2024 by Y. Michimura and M. Ando
Feasibility: 0 (Proposal of concept in 2012)

Vertical suspension point interferometer (VSPI) is an active vibration isolation scheme for vertical direction. It makes use of a vertically arranged interferometric sensor, such as a Fabry-Perot interferometer, between upper and lower stages of a test mass suspension. The differential motion of these stages caused by residual seismic motion or thermal noise of the suspension wire is

monitored by this interferometer called VSPI. The output of the VSPI is fed back to the upper stage with a gain G. Since the lower stage is quieter than the upper one, owing to the vibration isolation by the springs connecting them, this feedback reduces the vertical motion of the upper stage using the lower stage as an inertial reference.

The transfer function of the VSPI gives that the resonant frequency ω of the system is effectively reduced by a factor of $1/\sqrt{1+G}$ and the quality factor Q is increased by a factor of $\sqrt{1+G}$, where G is the gain of the lock. In this way, a very low vertical resonant frequency can be realized.

References:

- Masaki Ando, *Vertical Suspension-Point Interferometer*, JGW-G1201177 (2012).

3.6.6 Newtonian noise studies and cancellation

Version history: First version in 2024 by A. Nishizawa, adding to the paragraghs of water gravity gradient noise and atmospheric gravity gradient noise in the KAGRA+ white paper in 2019.

Feasibility: 2 (Demonstration experiment on going)

Gravity gradient noise, the so called Newtonian noise, is caused by time-varying gravitational potential generated by seismic waves, acoustic waves, air flows, water flows, and so on. The dominant source of the Newtonian noise depends on the target frequency band and the sensitivity in the band. For the KAGRA upgrade targeting at the frequencies above several Hz, the contributions from seismic waves, acoustic waves, and air flows would be subdominant and would not affect the design sensitivity of the KAGRA and KAGRA upgrade. The Newtonian noises from water flows and the cooling system might contaminate the sensitivity of the KAGRA upgrade and need more precise estimates of their spectra.

- Seismic Newtonian noise

  Seismic waves are classified into body waves and surface waves. Each is further devided into subcategories. The dominant contribution to the Newtonian noise from the body waves is s-waves and the one from the surface waves is Rayleigh waves [Harms 2019]. The s-waves exist everywhere underground, but the Rayleigh waves are more damped as the underground depth increases. The seismic Newtonian noise from body and surface waves have been estimated in [ET Design Report 2020] as Fig. 5. For the estimate, the typical magnitude of underground seismic spectra and the dispersion model (Rayleigh-wave speed of 1.8 km/s at 1 Hz and 500 m/s at 10 Hz) are assumed. The Newtonian noise from surface waves is depth-dependent and would be larger than that from body waves below several Hz for KAGRA located at 100–300 m from the surface of the mountain [Private communication with Yokozawa-san]. Above several Hz, the Newtonian noise from body waves dominates, but its contribution is

below the noise curve of ET. For KAGRA, the spectrum would be three times larger than that for ET due to the arm-length difference. However, the total Newtonian noise would not affect the sensitivity of the KAGRA upgrade unless the sensitive frequency band is extended down to several Hz. Note that the Newtonian noise spectra could be much larger if the underground seismic spectra and the dispersion model at the KAGRA site are not typical ones but significantly different from those assumed above. Such site dependence should be checked carefully.

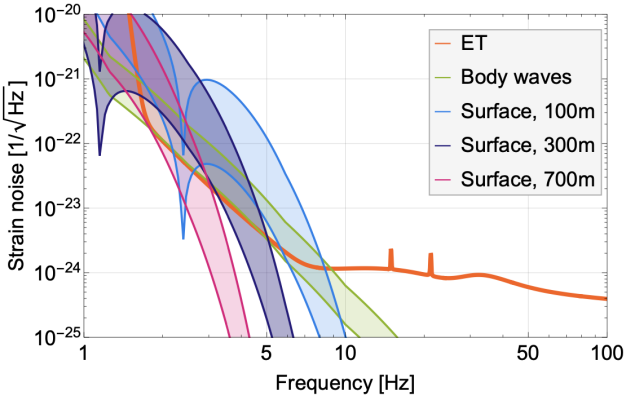

Figure 5: Estimates of seismic Newtonian noise for ET [ET Design Report 2020].

- Water Newtonian noise

  Vast amount of spring water comes up early spring in the Kamioka mine and the bumpy water flow would cause gravity gradient near test masses and low frequency noise. Total water flow can reach over 1000 tons per hour at the end of the drain pipe that starts from the X-end through the central area toward the Y-end. There are three types of drain pipe. One is with a pair of compulsory pumps located by the Y-arm about 1 km and 2 km from the center. This drain system can transport up to 400 t/h. Another is a bypass pipe starting 100 m before the Y-end. This pipe transports up to 450 t/h. The last one is a regular drain pipe that goes under the Y-end chamber. The largest concern is on the last one that reaches up to a few meter from the test mass. Chen and Nishizawa created a theoretical model based on an assumption that the water surface does not change its shape and flows in a constant speed, in which case the noise spectrum increases exponentially with the speed of the water flow [Nishizawa 2021]. The noise level, however, turns out to be below the KAGRA target sensitivity even if the speed is less than 5 m/s. In reality, water surface is not constant but changes in time. Even worse, turbulence is developed partially. The theoretical study shows that assuming the Kolmogorov's scaling law the spectral tilt of strain noise in $1/\sqrt{\mathrm{Hz}}$ is $f^{-17/6}$,

but it cannot fully deal with turbulent flows and predict its amplitude. To investigate the contribution from turbulent flows, numerical simulations have been performed [Suzuki 2021]. The simulation results showed the Newtonian noise would be smaller than the target sensitivity regardless of the amount of water flow. However, the noise level did not converge with the mesh size in the finite element analysis. Some more investigation is necessary.

- Atmospheric Newtonian noise

  Motion of molecules in the air around the test masses can cause Newtonian noise. The effect can be categorized to the contribution from the atmosphere outside the building, which is the dominant for ground-base detectors, and the contribution from the atmosphere inside the building/mine, which is the dominant for underground detectors. Reference [Fiorucci *et al.* 2018] shows that the atmospheric Newtonian noise would not limit the sensitivity of Advanced Virgo or of Einstein Telescope.

- Newtonian noise from the cooling system *First version in 2024 by Rishabh Bajpai*

  As mentioned in Sec. 3.4.2, while the underground location provides a quiet site with low seismic noise, the cooling infrastructure is known to generate large mechanical vibrations due to cryocooler operation and structural resonances of the cryostat. As cooling system components are relatively heavy and in close proximity to the test masses, oscillation of gravity force induced by their vibration, so-called Newtonian noise, could contaminate the detector sensitivity. Therefore, the Newtonian noise coupling from cryogenic components was evaluated and the results are summarized in [Bajpai *et al.* 2023]. It was found that the largest contribution to NN comes from the breadboard, followed by radiation shields, cryostat and the baffle. While the baffle is the closest object to TM, its NN contribution is the lowest because of vibration attenuation from the baffle suspension and relatively low mass. The results shown in [R. Bajpai *et al.* 2023] and fig 6 show the upper limit of the cooling system Newtonian Noise, i.e., the mode shapes of peaks due to resonances (like the largest peak at 21.8 Hz from shield resonance) are not taken into account and could cancel out. If the cooling system's Newtonian noise does turn out to be a problem, it can be eliminated by reducing the vibration of the cryocooler or removing heavy objects (like breadboard) from the cryostat. We could install stiffness plates or look into employing Wiener filters for NN from resonance modes.

- Newtonian noise cancellation and mitigation

References:

- J. Harms, Living Reviews in Relativity 22:6 (2019).

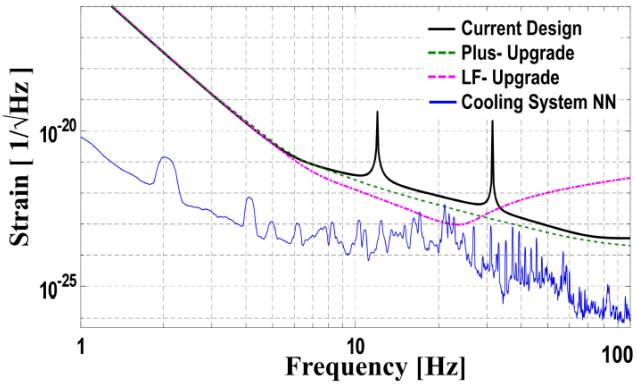

Figure 6: Comparison of current and upgraded KAGRA design sensitivity with calculated Cooling System Newtonian Noise.

- ET Steering Committee Editorial Team, Design Report Update 2020 for the Einstein Telescope (2020).
- A. Nishizawa, KAGRA internal document, "Water Newtonian noise for KAGRA", JGW-T1706440-v2 (2021).
- D. Fiorucci, J. Harms, M. Barsuglia, I. Fiori, and F. Paoletti, Phys. Rev. D 97, 062003 (2018).
- Bajpai *et al.*, Phys. Rev. D 107, 042001 (2023).
- R. Bajpai *et al.*, Proceedings of Science, TAUP 2023, 115 (2023).

3.6.7 Environmental magnetic noise sensors

Version history: First version in 2019 by Someone; Updated in Aug. 2024 by Yokozawa
Feasibility: 5 (monitors installation were already done, let't have a detector characterization)

There are several type of the magnetic noise in gravitational wave detector. Not only the KAGRA, but also LIGO and Virgo detectors had several magnetic noise. We can describe the following three categories.

1. Magnetic field from the instruments and circuits
2. Magnetic field from the power line and ground
3. Magnetic field from the phenomena, such as lightening

References:

- KAGRA Collaboration, Progress of Theoretical and Experimental Physics 2021, 05A101 (2021). item https://arxiv.org/pdf/1802.00885

3.6.8 Charge noise reduction

Version history: First version in November 2024 by T. Akutsu
Feasibility: 0 (Not clear for cryogenic sapphire mirrors)

The charging noise in the terrestrial GW detectors has been practically studied since prototyping the electrostatic actuator for LIGO at GEO600 [M. Hewitson et al. (2007)], in which more older researches can be found such as S. Rowan et al. (1997), which also discusses about the reduction of Q factors of fused silica material due to the charging. Some efforts to estimate the noise has been reported for initial, enhanced, and advanced LIGO [G. Harry ed. (2008)]. The noise effect is also discussed in the recent LIGO [Martynov et al. (2016), A. Buikema et al. (2020)], which estimates the charge density of the test mass surfaces as $\sim 10^{-11}\,\mathrm{C/cm^2}$, and says the dominant coupling would be that of the electro-statical force on the charged test mass and the electric field fluctuation around the mirror. The electric fluctuation might arise from voltage fluctuation of some metal structures ($\sim 1\,\mu\mathrm{V/Hz^{1/2}}$). Discharging the test mass would be the best way to reduce this coupling drastically, and in LIGO, they use ion guns [P. Campsie et al. (2011), D. Ugolini et al. (2014)]. Considering the fact that the fused silica is a dielectric material, using UV illumination might not work for discharging, but it seems not true [M. Hewitson et al. (2007)]. In the experiment and experience, the UV light may be usable to control the charging; discharging negative ones from the mirror with the direct illumination; compensate positive charges on the mirror by illuminating some metal materials around the mirror to generate some negative charges. To transmit the UV light effectively from the outside of the vacuum chamber, the dedicated window material should be like such material as fused silica, which would have the higher transmittance to the UV light.

In KAGRA, we have not yet evaluated this charging noise on the test masses. KAGRA dose not have a plan to install such discharging tools. Note that most (all) of the window materials around the test masses in KAGRA are made not of fused silica. Note that most of the studies so far (mentioned above) has been done for silica mirrors in room temperature, while KAGRA ones are of sapphire under the cryogenic environment. We are not sure the experience for the silica would be applicable. In the cryogenic environment, some particles, which may have some charges, would rapidly accumulate on the test mass surfaces [K. Hasegawa et al. (2019)]. Also, the accumulation rate might relate with what kind of coatings on the mirror.

KAGRA is so far not using the electrostatic actuators, so the charging rate on the mirror might differ from that of LIGO. But note that the main coupling path is irrelevant with whether the electrostatic actuators would be used or not. An interesting tip is pointed out by several references that the FirstContact cleaning will leave significant amount of charges on the mirror.

The following may be not directly related to the charging noise here, but it might be worth introducing it. In the LCGT design document, some noise due to cosmic rays are discussed, and the main particles under consideration was muons. The main conclusion was such cosmic rays may not be an issue in the

process considered. But it may be worth revisiting in the future.
References:

- M. Hewitson et al., "Charge measurement and mitigation for the main test masses of the GEO 600 gravitational wave observatory", Class. Quantum Grav. **24**, 6379 (2007)
- S. Rowan et al., "Investigations into the effects of electrostatic charge on the Q factor of a prototype fused silica suspension for use in gravitational wave detectors", Class. Quantum Grav. **14**, 1 (1997)
- G. Harry ed., "Estimate of Noise from Charging in Initial, Enhaced, and Advanced LIGO", LIGO-T080019-01-R (2008)
- D. V. Martynov et al., "Sensitivity of the Advanced LIGO detectors at the beginning of gravitational wave astronomy", Phys. Rev. D **93**, 112004 (2016)
- A. Buikema et al., "Sensitivity and performance of the Advanced LIGO detectors in the third observing run", Phys. Rev. D **102**, 062003 (2020)
- D. Ugolini et al., "Discharging fused silica optics occluded by electrostatic drive", Rev. Sci. Instrum. **85**, 034502 (2014)
- P. Campsie et al., "Charge mitigation techniques using glow and corona discharges for advanced gravitational wave detectors", Class. Quantum Grav. **28**, 215016 (2011)
- K. Hasegawa et al., "Molecular adsorbed layer formation on cooled mirrors and its impacts on cryogenic gravitational wave telescopes", Phys. Rev. D **99**, 022003 (2019)
- LCGT design document ver. 3.0, JGW-T0400030-v4 (2009)

3.6.9 Instrumented baffles

Version history: First version in November 2024 by T. Akutsu
Feasibility: 3 (Installed in LVK detectors, but still under study for scattered light noise mitigations)

So far KAGRA does not have a plan to develop the instrumented baffles any more. The narrow-angle baffles (NABs) of KAGRA, each of which has been installed at a few tens of meters away from the cryogenic test masses equips four photodiodes (PDs). Historically, this instrumentation was not in the scope of the original plan of the NABs. Around 2017-2018, it was a sudden thing to add these PDs. Modification of the already complex system was a tough thing. Unfortunately, currently they are not used at all.

There is a tip for the person who will develop this kind of instrumentation in the future; the electric wires from the PDs easily vary the NAB suspension's

resonant frequencies and Q values if improperly treated, so please be careful. See the relevant klog posts.

Note also that, since some ray-trace simulation in the past for KAGRA (see the relevant JGWdocs), we have known that the main scattering sources in the arm cavity structure is indeed the structure around the NAB. Nowadays, they may include Pcal structures, TCam structures, and also the instrumentation PDs. We may need to revisit this issue when the sensitivity of KAGRA will get more better.

In LIGO, each of "arm cavity baffles" (ACBs) equips some PDs. As long as I have heard, these PDs are sometimes used for the initial alignment of the main laser beam axis by checking the scattered out light from the test masses. In fact, one interesting application of these PDs are to monitor the scattering light to study the currently-used mirror quality. See the LIGO documents in the reference.

In Virgo, they actively develop such instrumental baffles. For example, cool photos of them can be found in the web. For example, one of such baffles has been installed at the suspended end mirror of the input mode cleaner of Virgo; see the PRD paper in the reference.

References:

- W. Jia et al., "Physical and Statistical Analysis of Scatter in Fabry-Pérot Arm Cavity of Advanced LIGO" LIGO-T1800224-v1 (2018).
- H. Yamamoto, "BRDF revisited" LIGO-T2400308-v1 (2024).
- M. Andrés-Carcasona et al., "Instrumented baffle for the Advanced Virgo input mode cleaner end mirror", Phys. Rev. D **107**, 062001 (2023)

3.7 Study of New Noise Sources

3.7.1 Schumann resonance

Version history: First version in 2024 by T.Yokozawa240921
Feasibility: **5** (LKV continuously measured the Schumann resonance and study of the effect for the SGWB search)

Schumann resonance is the resonance of the Earth electromagnetic field between the ionopshere and the Earth surface. The 1st mode is about 8 Hz, 2nd and 3rd mode are about 14 Hz and 20 Hz, respectively. This resonance are generated by the interaction of the lightening discharges. The global magnetic noise can be a backgound for the SGWB search, so we need to investigate the long term correlation between the LIGO, Virgo and KAGRA. The global correlation was already investigated in the past measurements. But one of the mysterious result in KAGRA is the amplitude of measured Schumann resonance inside the mine was quite larger than that of the outside the mine. That was the long mystery, but when we measured the Schumann resonance very close to the 3 km arm, the amplifier of the amplitude was detected. We also investigated the Virgo site and CLIO cite. Also, the vector of the magnetic field was circular for

the tube suface, the amplidtude was reduced in the distance. Long term observation of the Schumann resonance would support the SGWB search, but almost all things were already achieved in KAGRA experimental area. All results for Schumann resnonce can be found in reference.
References:

- S.Atsuta etal, "Measurement of Schumann Resonance at Kamioka", J. Phys.: Conf. Ser. 716 012020 (2016).
- JGWDoc13227
- JGWDoc13120
- JGWDoc14203
- JGWDoc14297
- JGWDoc14514
- JGWDoc14553
- JGWDoc14841
- JGWDoc14868
- JGWDoc14757
- JGWDoc15066
- JGWDoc15360
- JGWDoc15362
- JGWDoc15377

3.7.2 Thermal noise in non-equilibrium steady state

Version history: First version in Nov. 6th, 2024 by KK
Feasibility: 3 (A. Fontana demonstrated with a table-top in 2021)

In the context of GW detectors, thermal noise is often described by the fluctuation-dissipation theorem (FDT) under equilibrium conditions, assuming a constant temperature across the system. However, in systems where cryogenic cooling is employed, such as in the KAGRA, the temperature distribution becomes non-uniform. This non-equilibrium condition makes it challenging to apply traditional models of thermal noise, which typically assume a homogeneous temperature distribution throughout the suspension system.

To address this limitation, a generalized form of the FDT has been derived to accommodate locally varying temperature profiles within the suspension system [Komori *et al.*2019]. This approach allows the FDT to be applied in a non-equilibrium setting, where each part of the suspension system can be at a

different temperature, as is the case in KAGRA's cryogenic setup with temperature gradients. To the first approximation, the average temperature within the suspension fiber can be used to estimate thermal noise by applying conventional equations under these modified assumptions. Some experimental studies have validated this approach using mechanical oscillators with significant thermal gradients [Fontana *et al.*2021, Shaniv *et al.*2023].

The application of the non-equilibrium FDT to thermo-elastic and thermo-refractive noise is a promising but challenging future direction. The primary difficulty lies in calculating temperature fluctuations in the presence of temperature gradients, as these gradients introduce complexities beyond conventional equilibrium assumptions. In non-equilibrium conditions, temperature variations can be substantial, making the standard linear approximation for heat flow insufficient for the entire system. Furthermore, maintaining a steady temperature gradient inherently causes stationary thermal dissipation, complicating the isolation of noise relevant to the fluctuation-dissipation theorem. Addressing these issues is essential for accurately estimating thermo-elastic and thermo-refractive noise, making this a critical area for future research.

References:

- K. Komori *et al.*, Phys. Rev. D 97, 102001 (2019).
- A. Fontana *et al.*, Phys. Rev. E 103, 062125 (2021).
- R. Shaniv *et al.*, Phys. Rev. Research 5, 043121 (2023).

3.7.3 Gravitational Decoherence Noise

Version history: First version in 2019 version (JGW-M1909590); Update is in progress by Jyotirmaya Mohanta in 2024.

Feasibility: 0 (Theoretical Study is on going)

Quantum mechanics is experimentally confirmed to be valid in microscopic system while not in macroscopic one. One of the solution to this issue is non-linear term in Schrödinger equation resulting in the spontaneous wave-function collapse for massive degrees of freedom [A. Bassi, et al. 2017]. The collapse causes momentum diffusion of the mechanical mode and generates a random noise. It could set a fundamental limit on detector sensitivities. The collapse model which has been discussed and tested the most is continuous spontaneous localization (CSL) model [G. C. Ghirardi et al. 1990]. The noise spectrum is flat in the unit of force spectral density. The amplitude is determined by two phenomenological parameters of a characteristic length and a collapse rate. Some areas in the parameter space were excluded by precise measurement experiments using a SQUID cantilever [A. Vinante et al. 2017] and GW detectors of aLIGO and LISA path finder [M. Carlesso et al. 2016].

References:

- Angelo Bassi et al., Gravitational Decoherence, Class. Quantum Grav. 34 193002 (2017).

- G. C. Ghirardi et al., Markov processes in Hilbert space and continuous spontaneous localization of systems of identical particles, Phys. Rev. A 42, 78 – Published 1 July 1990.
- A. Vinante et al., Improved Noninterferometric Test of Collapse Models Using Ultracold Cantilevers, Phys. Rev. Lett. 119, 110401 – Published 12 September 2017.
- M. Carlesso et al., Experimental bounds on collapse models from gravitational wave detectors, Phys. Rev. D 94, 124036 – Published 23 December 2016.

3.8 Advanced classical control systems

3.8.1 Phase camera

Version history: First version in October 2024 by S. Tanioka
Feasibility: 5 (3 for the polarization phase camera) (Demonstrated in Advanced LIGO and Adcanced Virgo)

Phase cameras are often used for diagnostic purpose because they can produce image maps of the transverse amplitude and phase of optical beat notes between frequency shifted two beams. Scanning pinhole phase cameras have been significantly developed [K. Agatsuma *et al.* 2019]. In this scheme, either the test beam, or both test and reference beams are scanned by a piezo transducer, and beat notes are demodulated I- and Q-phases. This phase camera is routinely used in Advanced Virgo [L. van der Schaaf *et al.* 2016], and can be utilized for mode-matching control [R. Cabrita *et al.* 2024].

Optical lock-in phase cameras use amplitude modulation by a Pockels cell in order to optically demodulate the RF beat down to DC frequency [H. T. Cao *et al.* 2020]. With this optical lock-in phase camera, one can image parametric instabilities (PIs), and determine the mode of PI [M. Schiworski *et al.* 2022].

Time-of-flight (ToF) phase cameras also have been developed [E. Muniz *et al.* 2021]. ToF phase camera is capable of sensing optical path distortions at the order of nanometer, which enables to detect point absorbers in the test masses.

Recently, a polarization phase camera is being demonstrated at Cardiff University [T. Pearce 2023]. This scheme utilize the scanning pinhole phase camera with an additional PBS and a PD. Once this phase camera is commissioned, one can image the in-situ birefringence map of sapphire test masses.
References:

- K. Agatsuma *et al.*, Optics Express **27**, 18533-18548 (2019)
- L. van der Schaaf *et al.*, J. Phys. Conf. Ser. **718**, 072008 (2016)
- R. Cabrita *et al.*, Nuclear Inst. and Methods in Physics Research, A **1068**, 169806 (2024)
- H. T. Cao *et al.*, Optical Express **28**, 14405-14413 (2020)

- M. Schiworski *et al.*, Optics Letters **47**, 1685-1688 (2022)
- E. Muniz *et al.*, Physical Review D **104**, 042002 (2021)
- T. Pearce, *Polarisation Phase Camera*, LIGO-G2300545 (2023)

3.8.2 Machine learning

Version history: First version in October 2024 by Y. Michimura
Feasibility: 5 (Already applied in many ways to LVK detectors)

Machine learning have been used in the field of gravitational waves in many ways such as data analysis, noise subtraction, detector characterization, suspension damping and interferometer controls. Human learning based, classical and simple linear methods often work pretty good and machine learning would not help improving over such methods. For example, the matched filter is the optimal linear filter for maximizing the signal-to-noise ratio when dealing with stationary Gaussian noise. Machine learning could have a potential for improving things when the system is nonlinear or nonstationary. One example is the use of machine learning for nonlinear suspension local controls. Another example is the use of deep learning for subtracting noises that have non-linear, and non-stationary coupling mechanisms [Ormiston 2020]. Human also have discovered new interferometer configurations working with artificial intelligence [Krenn 2023].

References:

- R. Ormiston *et al.*, Phys. Rev. Research 2, 033066 (2020).
- M. Krenn *et al.*, arXiv:2312.04258.

3.8.3 Noise subtraction methods

Version history: First version in October 2024 by Y. Michimura
Feasibility: 5 (Already applied in many ways to LVK detectors)

Noises in the $h(t)$ data can be subtracted when the noises are monitored by witness sensors which do not see gravitational-wave signals. Wiener filtering [Driggers 2019] or deep learning based approaches (DeepClean) [Ormiston 2020] have been widely used in LIGO and Virgo. Independent conponent analysis based methods were also applied for KAGRA data [KAGRA 2020, KAGRA 2023]. More studies are ongoing for data cleaning of nonlinear and nonstationary noises.

References:

- J. C. Driggers *et al.*, Phys. Rev. D 99, 042001 (2019).
- R. Ormiston *et al.*, Phys. Rev. Research 2, 033066 (2020).
- KAGRA Collab. PTEP 2020, 053F01 (2020).
- KAGRA Collab. CQG 40, 085015 (2023).

3.8.4 Laser induced desorption

Version history: First version in 2019 by K. Hasegawa; Summarized in September 2024 by S. Tanioka
Feasibility: **0** (Idea phase)

Employing cryogenically cooled mirrors as test masses in a gravitational wave detector (GWD) can reduce the thermal noise arises from the mirror substrate and its coatings. However, such cryogenic mirrors can suffer from the formation of ice layers on their surfaces, which degrade the performance of the GWD [Hasegawa *et al.* 2019]. A laser-induced desorption of the ice layers is a possible solution for the ice layer formation to enable long-term operation. There are two laser desorption methods; the non-thermal desorption with a UV laser, and the thermal desorption with an IR laser.

The thermal desorption method increases the energy of the molecules so that they *escape* from the biding energy of the surfaces. This desorption process follows Arrhenius equation as

$$-\frac{dN_{\rm s}}{dT} = \frac{k_{\rm d}(N_{\rm s})^m}{\beta}\exp\left(-\frac{E_{\rm des}}{k_{\rm B}T}\right), \tag{1}$$

where $N_{\rm s}$ is the number of molecules on the surface in a unit area, m is the order of the reaction, $E_{\rm des}$ is the desorption energy, $k_{\rm B}$ is the boltzmann constant and T is the temperature. The desorption energy of H_2O molecules, which is the main vacuum residual gas and has the large desorption energy, is $E_{\rm des} \sim 50\,{\rm kJ/mol}$ [Shakeel *et al.* 2018, Thiel *et al.* 1987]. Assuming $m = 0$ and $k_{\rm d} \sim 10^{30}$, the temperature needs to reach higher than 170 K as shown in Fig. 7 in order to desorb the H_2O molecule with 300 μm thickness and the heating speed of $\beta = 0.1\,{\rm K/s}$. Such heat treatment may be achieved by illuminating the test mass with a CO_2 laser, for instance, an idea proposed for preheating aLIGO test masses [V. Jaberian Hamedan *et al.* 2018]. Recently this scheme is under R&D, called CHETA [C. Compton *et al.* 2023]

The non-thermal desorption method excites the electron and cut the binding between molecules. This technique has been studied in the vacuum technology. For instance, a certain wavelength of high power pulsed laser which is strongly absorbed by the only frost can increase the temperature of the frost enough to sublime within an order of 100 ns or 1 μs [Takeuchi *et al.* 1992]. Ref. [Takeuchi *et al.* 1992] observed the desorption process using a pulse laser ($P_0 = 2\,{\rm MW}$, $\lambda_0 = 1064\,{\rm nm}$, pulse width $\sim 10\,{\rm ns}$, and beam size $w_0 \sim 3\,{\rm mm}$) and heating the metal surface. However, as shown in Ref. [Nettesheim *et al.* 1996], it needs laser intensity of about $10\,{\rm MW/cm^2}$, and it can cause damage on the mirror and coatings if the laser reaches the mirror surface through the frost.

In order to realize a laser induced desorption system in a cryogenic gravitational wave detector, further design studies including theoretical calculation and simulation are necessary. Based on those studies, we should develop a tabletop setup to verify the system which relies on either thermal or non-thermal process.

References:

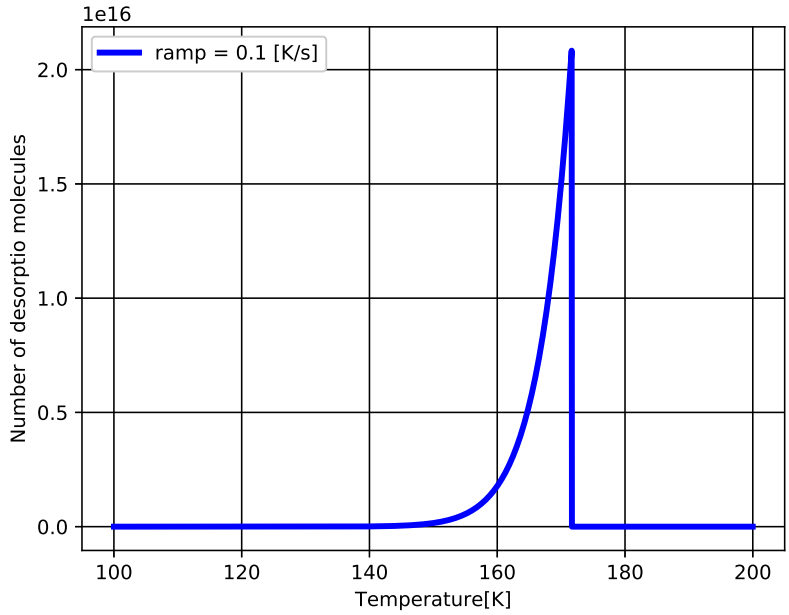

Figure 7: Desorption spectrum of H_2O molecules. The parameters for this calculation are $E_{\rm des} = 0.5\,{\rm eV}$ and $\beta = 0.1\,{\rm K/s}$. The number of initial absorbed molecules is assumed to be $10^{19}\,1/{\rm mm}^2$ which is equivalent to the frost thickness of about $300\,\mu{\rm m}$.

- K. Hasegawa *et al.*, Physical Review D **99**, 022003 (2019)
- H. Shakeel *et al.*, The Journal of Chemical Thermodaynamics **118**, 127-138 (2018)
- P. A. Thiel and T. E. Madey, Surface Science Reports **7** 211-385 (1987)
- V. Jaberian Hamedan *et al.*, Classical Quantum Gravity **35**, 115006 (2018)
- C. Compton *et al.*, *CHETA Document of Requirements*, LIGO-T2300387 (2023)
- K. Takeuchi *et al.*, Shinku **35** 837-844 (1992)
- S. Nettesheim and R. Zenobi, Chemical Physics Letters **255** 39-44 (1996)

3.8.5 Quantum locking

Version history: First version in 2019 by K. Nagano; Updated and summarized in August 2024 by Y. Michimura

Feasibility: 3 (T. Ishikawa demonstrated with a table-top in 2023)

Quantum locking [Courty *et al.*2020, Heidman *et al.*2004] is based on active control of the motion of a mirror which is main test mass of the gravitational wave detector using a short auxiliary cavity. Within the controlled frequency range, the main mirror follows to the auxiliary mirror motion of which noise should be quantum noise level (or, at least, better than main mirror's noise level in terms of displacement). This technique widens the strain sensitivity to the lower frequency band. When the displacement noise of the main test mass is limited by the radiation pressure noise, quantum locking can be used to reduce it.

For application in KAGRA, we should solve challenges of the auxiliary cavity sensitivity and facility. In order to suppress the radiation pressure noise of the main cavity, we need the auxiliary cavity whose displacement noise is smaller than that of the main cavity around 50 Hz. It could also be difficult to host auxiliary cavity, especially in X-end station. Table-top demonstration in the classical regime targeted for application in DECIGO was reported in [Ishikawa *et al.*(2023)].

References:

- J. M. Courty, A. Heidmann, and M. Pinard, Phys. Rev. Lett. 90, 083601 (2003).
- A. Heidmann, J.-M. Courty, M. Pinard, and J. Lebars, J. Opt. B 6, S684 (2004).
- T. Ishikawa *et al.*, Phys. Rev. D 107, 022007 (2023).

3.9 Quantum control systems

3.9.1 Homodyne readout

Version history: First version in WP2019; Updated in August 2024 by K. Somiya

Feasibility: 3 (Demonstrated by N. Aggarwal in 2020)

Quantum radiation pressure noise (QRPN) comes from the quantum fluctuation of vacuum field in the amplitude quadrature. Tuning the readout quadrature using either a balanced homodyne detector [Kimble 2001, Fritschel 2014] or a DC readout scheme with finite offset [Somiya 2006], QRPN can be cancelled and the quantum noise spectrum exceeds SQL at around a certain frequency to reach the shot noise level.

References:

- J. Kimble *et al.*, Phys. Rev. D **65**, 022002 (2001).
- P. Fritschel *et al.*, Opt. Express **22**, 4224-4234 (2014).
- K. Somiya *et al.*, Phys. Rev. D **73**, 122005 (2006).
- N. Aggarwal *et al.*, Nat. Phys. **16**, 784-788 (2020).

3.9.2 Variational readout

Version history: First version in WP2019; Updated in August 2024 by K. Somiya
Feasibility: 2 (Technological challenges should be common to FDSQ)

Homodyne detection with a fixed but non-zero homodyne angle realizes a cancellation of quantum radiation pressure noise (QRPN) at around a certain frequency. Using an output filter cavity, which is a similar optical cavity as the one used for frequency dependent squeezing, QRPN can be cancelled at all the frequencies. Ideally, the quantum noise spectrum coincides to the one of shot noise, but in practice the influence of optical losses degrades the sensitivity.
References:

- J. Kimble *et al.*, Phys. Rev. D **65**, 022002 (2001).

3.9.3 Optical spring

Version history: No section in the version 2019; First version in 2024 by K.Somiya
Feasibility: 4

By detuning an optical cavity, a phase modulation signal converts to a mixed modulation with some fraction of amplitude modulation component that couples with the input carrier field to generate power fluctuation. The power fluctuation inside the cavity generates radiation pressure to displace the test masses. This optomechanical loop leads to form an *optical spring* [Buonanno and Chen 2001]. The optical spring amplifies the gravitational wave signal and also squeezes the vacuum field from the dark port. Because of the non-zero correlation between the amplitude and phase fluctuations of the vacuum field, the quantum noise spectrum exceeds the free-mass SQL. The signal amplification with the optical spring is a classical effect so that it can be observed in a transfer function measurement [Miyakawa 2006]. Either the real part or the imaginary part of the single optical spring must be negative. For the signal amplification, the real part must be positive, so the imaginary part is negative and it requires a classical feed back control at the resonant frequency to avoid instability. In 2007, Chen proposed to combine two optical springs to have both real and imaginary parts positive, and the idea was demonstrated at MIT [Corbitt 2007].
References:

- A.Buonanno and Y.Chen, Phys. Rev. D, 64, 042006 (2001)
- O.Miyakawa *et al.*, Phys. Rev. D, 74, 022001 (2006)
- T.Corbitt *et al.*, Phys. Rev. Lett., 98, 150802 (2007)

3.9.4 Long-SRC

Version history: First version in 2019 by K. Somiya; Updated in October 2024 by K. Somiya

Feasibility: 3 (Demonstrated by K. Komori in 2024)

When the signal-recyling cavity (SRC) is set resonant for the carrier light at DC, the signal recycling gain decreases at low frequencies and increases at frequencies higher than the cavity pole. This can be explained by the sign flip of the real part of the arm cavity reflectivity at the cavity pole. The sign flip of the real part alone does not help removing the influence of the phase delay, but the imaginary part can be also compensated by the use of a delay line in the SRC. At a certain frequency, the phase delay in the arm cavity can be compensated by the phase delay in the SRC, and then the quantum noise spectrum shows a dip at around the frequency. This is called the Long-SRC effect.

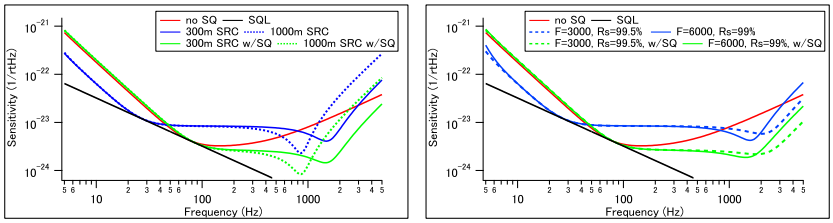

Figure 8: Sensitivity curve of KAGRA with a long signal recycling cavity and frequency-independent squeezing.

Example spectra are shown in Fig. 8 (Figures 11 and 12 of [K. Somiya (2020)]). By changing the SRC length from the original 66 m to 300 m, the shot noise curve shows a dip at around 2 kHz. A dip at 2 kHz can be realized without extending the SRC but with increasing the arm cavity finesse and the signal recycling mirror (SRM) reflectivities.

Since there is no asymmetry in the upper and lower signal sidebands, the squeezing angle does not rotate at around the dip frequency. Thus, unlike the squeezing of a detuned interferometer, a simple frequency independent squeezing is good enough to obtain a gain in broadband frequencies around the dip frequency.

The LSRC technique has been proposed for NEMO. The same technique with a high reflectivity SRM, proposed in [K. Somiya (2020)] has been favored by the KAGRA 10-year taskforce.

References:

- H. Miao *et al.*, Class. Quantum Grav. **31**, 165010 (2014).
- K. Somiya, Eur. Phys. J. D **74**, 10 (2020).

3.9.5 Quantum expander

Version history: Not present in 2019 paper; Updated in July 2024 by M. Page
Feasibility: 2 (Theoretical papers written by [M. Korobko *et al.*(2019)] and [V. Adya *et al.*(2020)]. Development of internal squeezing techniques ongoing

at Australian National University, University of Hamburg, Tokyo Institute of Technology.)

The quantum expander is an idea proposed by [M. Korobko *et al.*(2019)] for optically enhancing the bandwidth of a gravitational wave detector. The idea was extended to long signal recycling detectors by [V. Adya *et al.*(2020)]. The main motivation is to increase the sensitivity to high frequency neutron star mergers without compromising the sensitivity to other signals.

The quantum expander concept is based on the internal squeezing technique, where an optical parametric amplifier is pumped inside the signal recycling cavity. The ultimate sensitivity of a detector is limited by the Quantum Cramer-Rao Bound, which, broadly speaking, dictates that increasing the radiation pressure force on the test mass increases the uncertainty of momentum but makes position measurement more precise. Amplifying the radiation pressure fluctuations at the signal frequency has been previously explored using coupled resonators or negative dispersion media. In the quantum expander scheme, the respective amplification is achieved by pumping a nonlinear crystal inside the signal recycling cavity. The signal recycling cavity itself is operated in signal extraction mode - close to the carrier resonance, signal sidebands are anti-resonant, so almost no squeezing occurs, while further from the carrier resonance, the quantum amplitude and phase fluctuations are squeezed. The radiation pressure noise increase (shot noise reduction) balances the signal reduction for high frequency GW signals that are out of the arm cavity band, resulting in signal-to-noise ratio improvement at high GW frequencies.

The technical feasibility of the quantum expander is limited by the general challenges facing internal squeezing in a gravitational wave detector. The key issues are mode matching the large interferometer beam to a small nonlinear crystal and managing the green pump injection and extraction from the signal recycling cavity. Spurious OPA seeding and scattered light are critical issues for external squeezing in GW detectors, and internal squeezing would be expected to face the same issues. Development of internal squeezing technology has been ongoing for many years at University of Hamburg, and recently Australian National University and Tokyo Institute of Technology (now Institute of Science Tokyo) have started work on internal squeezing.

References:

- M. Korobko *et al.*, Light: Science and Applications 8, 118 (2019).
- V. Adya *et al.*, Classical and Quantum Gravity 37, 07LT02 (2020)

3.9.6 Intracavity OPA

Version history: First version in 2024 by K.Somiya

Feasibility: 3

The optical spring frequency in the detuned signal-recycled Michelson inter-

ferometer is given by

$$\Omega_{\rm os} = \sqrt{\frac{2\omega_0 I_{\rm BS}}{mc^2}\frac{2r_s\sin 2\phi}{1+r_s^2-2r_s\cos 2\phi}}, \quad (2)$$

where ω_0, $I_{\rm BS}$, m, c, r_s, and ϕ are the light angular velocity, laser power at BS, mass, speed of light, the amplitude reflectivity of the signal-recycling mirror, and the detune phase of the recycling cavity. The denominator of the second part inside the square root is always larger than unity.

By inserting an optical parametric amplifier (OPA) in the signal recycling cavity, the equation is replaced by the following equation.

$$\Omega_{\rm os}^{\rm PA} = \sqrt{\frac{2\omega_0 I_{\rm BS}}{mc^2}\frac{(s+1/s)\sin 2\phi - |s-1/s|}{(r_s+1/r_s)-(s+1/s)\cos 2\phi}}. \quad (3)$$

Here the relative phase of OPA is set to selected to maximize the spring frequency. One can see that the denominator of the second part inside the bracket can be zero (or negative, when the interferometer makes unstable), resulting in the infinitely stiff optical spring [Somiya 2016]. Tuning the parameters to have the optical spring at around 3-4 kHz, the sensitivity of the interferometer can be sensitive to observe the neutron star remnant, for example. This intracavity signal amplification technique is one of the possible upgrade plans.

References:

- K.Somiya *et al.*, Phys. Lett. A, 380, 521 (2016)

3.9.7 White-light cavity

Version history: First version in 2019; Updated in July 2024 by M. Page
Feasibility: 2 Shown to be feasible for gravitational wave detection in papers by H. Miao (2015, 2018), X. Li (2020), M. Page (2021). Tabletop experiments to demonstrate the required opto-mechanical filter cavity are ongoing at University of Western Australia (C. Zhao, C. Blair) and University of Birmingham (D. Martynov).

A white light cavity is named so for its original concept by Weis et al. [506] to make light with any wavelength resonate in a cavity using gratings inside. The original idea turned out to be unfeasible for gravitational wave detection, but Miao et al. found another way to realize a white light cavity using an unstable filter inside the signal recycling cavity [507]. A cryogenic micro-resonator works as an intracavity filter that compensates the phase delay of the field resonating in the signal recycling cavity so that the cavity pole can be pushed to higher frequencies. However, thermal fluctuation of the micro-resonator can dominate the phase delay compensation. A micro-resonator with mechanical quality factor of order 10^9 is required to keep thermal fluctuations from destroying the gravitational wave signal.

The intracavity filter requires a blue detuned pump beam to create a three mode interaction between the micro-resonator and gravitational wave sideband.

Such a scheme is inherently unstable, though the original concept paper of Miao showed that it is in principle controllable, and X. Li showed a signal readout idea can arrange the flow of energy to prevent mechanical ring-up (see section regarding PT symmetry).

The white light cavity concept has been shown in principle to be able to provide broadband signal-to-noise ratio enhancement by using a filter cavity with existing opto-mechanical elements. Namely, these technologies are:

- i) commercial 50nm thick Si_3N_4 membranes that have been used in quantum limited measurement,
- ii) micropendulum with soft mechanical suspension placed in an optical spring, such that the majority of the restoring force is provided by the lossless electromagnetic field,
- iii) shielding of a mechanical resonator from the external thermal bath using a 2-dimensional meta-material array which is constructed to have a phononic bandgap in a small band around the eigenfrequency,
- iv) plano-convex acoustic lens that geometrically prevents dissipation of mechanical energy.

The University of Birmingham aims to demonstrate the required filtering effect using i), while the University of Western Australia is working on ii)-iv). However, the combined difficulties of achieving practical thermal noise reduction, strong optomechanical coupling and mechanical mode stability are such that the idea has not progressed past proof-of-concept in a tabletop experiment.

References:

- M. Korobko et al., Light: Science and Applications 8, 118 (2019).

3.9.8 PT symmetry

Version history: Not present in 2019 paper; Updated in July 2024 by M. Page
Feasibility: 2 (Theoretical paper written by X. Li (2020). Experimental demonstration ongoing at University of Birmingham using design of J. Smetana (2023).)

PT symmetry is an idea proposed by X. Li *et al.*(2021) to create stable broadband quantum signal amplification in gravitational wave detection. The scheme is named after a general concept that is used in the study of quantum open systems using PT symmetric Hamiltonians. In the context of gravitational wave detection PT symmetry is applied as an extension of the white light cavity concept. High frequency gravitational wave signals exceed the cavity pole of the detector and acquire a phase delay. The white light cavity should apply a frequency dependent phase compensation that increases with frequency, which in essence is a negative dispersion effect. The Kramers-Kronig relations from linear response theory dictate that negative dispersion is not possible for stable systems, so necessarily negative dispersion requires an unstable system.

The PT symmetry scheme of Li places the signal readout in a separate optical mode $\hat{b}$ from that of the interferometer carrier $\hat{a}$. The interferometer carrier mode couples to the negative dispersion filter via a coupling rate G, while the optical signal is read out at a sloshing rate γ. If the input and output rates G and γ are perfectly balanced, we can evade instability of the negative dispersion filter.

The University of Birmingham is working on the demonstration of self-stable broadband quantum amplification according to a design paper by J. Smetana. One of the main limitations of optomechanical filter techniques in GW detectors is that the contribution of thermal noise must be kept at $T/Q_{\rm m} < 10^{-9}$, where $Q_{\rm m}$ is the quality factor of the mechanical resonator used to achieve amplification [H. Miao *et al.*2015], while also maintaining strong optomechanical coupling. The Birmingham experiment uses a cavity design such that quantum amplification could be demonstrated for $T/Q_{\rm m}$ 10^{-7}, allowing for easier development of the working principle.

References:

- X. Li *et al.*2021, Phys. Rev. D 103 122001 (2021)
- J. Smetana *et al.*2023, Phys. Rev. A 107, 043701 (2023)
- H. Miao *et al.*2015, Phys. Rev. Lett. 115, 211104 (2015).

3.9.9 Kerr amplification

Version history: First version in 2024 by K.Somiya
Feasibility: 2

An optical Kerr effect is a third-order non-linear effect that changes the refractive index n_0 of the material that the light transmits through to $n_0 + nI$ with n a material-dependent coefficient and I the intensity. The effect is non-zero for most materials but is very weak and negligible. A cascaded Kerr effect is another non-linear effect that can be observed with a second order non-linear crystal like KTP or LN when its temperature is tuned to the phase mismatching condition. Either Kerr effect is known to squeeze the light field. If we insert such a media in the arm cavity, the quantum noise sensitivity changes with the parametric amplification [Otabe 2024].

References:

- S.Otabe *et al.*, Phys. Rev. Lett. 132, 143602 (2024)

3.9.10 Photo-thermal effect

Version history: First version in 2024 by K.Somiya
Feasibility: 2

If the laser beam transmits through a medium, the optical path length changes with the thermal expansion and dn/dT. This photo-thermal effect appears differently when the cavity mirror moves toward the resonance or moves out from the resonance, making the spectrum asymmetric. The photo-thermal

effect is negligible at high frequencies but it matters at low frequencies. When the cavity is detuned, the photo-thermal effect changes both the real and imaginary parts of the optical spring. While a single positive optical spring is known to be unstable with a negative imaginary part, the photo-thermal effect can stabilize the optical spring.
References:

- J.Chow *et al.*, Opt.Lett., 30, 708-710 (2005)
- S.Otabe *et al.*, Opt.Express, 30, 42579-42593 (2022)

3.9.11 EPR squeezing

Version history: First version in 2019 by K. Komori, second version in 2024 by Y. Nishino.
Feasibility: 3 (ANU squeezing group and Hamburg's quantum group have demonstrated in 2020.)

Quantum noise is reduced below the standard quantum limit by a method using Einstein–Podolsky–Rosen (EPR)-entangled signals and idler beams. The method was proposed by Ma et al. in 2017 [Nat. Phys. 13, 776-780 (2017)]. Broadband reduction of quantum noise is realized even without an additional filter cavity. Two EPR-entangled beams are created: the signal beam around the carrier frequency, and the idler beam detuned by a few MHz. This idler beam experiences frequency-dependent quadrature rotation. In other words, we use an arm cavity itself as a filter cavity. Mainly input and readout losses determine the sensitivity limit of this scheme. The effect of these losses are doubled compared to the conventional method with the external filter cavity because two beams have the same amount of the losses. We get around 6 dB broadband improvement of quantum noises with their losses of 5%, which is promising in the near future.
References:

- Y. Ma, et al., Nature Phys 13, 776–780 (2017).
- Südbeck, J., et al., Nat. Photonics 14, 240–244 (2020)..
- Yap, M.J., et al., Nat. Photonics 14, 223–226 (2020)..

3.9.12 Quantum teleportation

Version history: First version in 2024 by Y. Nishino.
Feasibility: 1

Quantum teleportation squeezing is a implementation of quantum teleportation into gravitational-wave detectors. Through the protocol, one can provide arbitrary number of squeezing angle rotation equivalent to passive optical cavities. Advantages are 1) one does not need additional filter cavities. 2) less contribution of filter losses and 3) less contribution of filters' phase noise to sensitivity

by utilizing the stable and low-loss arm cavity as filter cavities. Drawbacks are the threefold contribution of input and output losses to the sensitivity.
References:

- Y. Nishino, et al., Phys. Rev. A 110, 022601.

3.9.13 Negative effective mass

Version history: First version in 2024 by K.Somiya
Feasibility: 1

This is an idea to use two entangled beams of light, probing the GWD and an auxiliary atomic spin ensemble, respectively. The latter plays the role of a free negative mass [Khalili 2018]. Combining the two light, the sensitivity can exceed SQL.
References:

- F.Khalili and E.Polzik, Phys. Rev. Lett. 121, 031101 (2018)

3.10 Alternative topologies

3.10.1 Speed-meter

Version history: First version in 2019 by K. Komori, second version in 2024 by Y. Nishino.
Feasibility: 1

A speedmeter is other ways to reduce quantum radiation pressure noise without increasing shot noise, that is, beat the conventional standard quantum limit. A Sagnac interferometer can measure relative momentum, or speed, of the test masses. The back-action noise can be evaded in measurement on the speed because it is a kind of QND observable. One type of configuration for the speed meter has two ring cavities as end mirrors of Sagnac interferometer [Phys. Rev. D 67, 122004]. The experimental demonstration was planned by Gräf et al. in 2014 [Class. Quantum Grav. 31 215009] and was planned to be demonstrated in University of Glasgow [arXiv:1603.07756].

Another design is based on polarization [Light Sci Appl 7, 11 (2018)] and [Physics Letters A, 382, 33, 2018, 2219-2225]. By circulating two orthogonal polarization in the interferometer simultaneously, and make them destructively interfere with each other, one can extract first derivative of phase which is proportional to the velocity of the test masses. This polarization-based speed meter is currently under demonstration in Maastricht University and National Astronomical Observatory of Japan [Phys. Rev. D 107, 084029].
References:

- Y. Chen, Phys. Rev. D 67, 122004.
- C. Gräf, et al., Class. Quantum Grav. 31 215009.
- S. S. Leavey, et al., arXiv:1603.07756.

- S. L. Danilishin, et al., Light Sci Appl 7, 11 (2018)..
- E. Knyazev, et al., Physics Letters A, 382, 33, 2018, 2219-2225.
- Y. Nishino, et al., Phys. Rev. D 107, 084029.

3.10.2 Acceleration-meter

Version history: First version in 2024 by Y. Nishino.
Feasibility: 1

Acceleration meter is an extension of speed meters. Instead of measuring velocity of mirrors, one measures their acceleration. This can be realized with a combination of two speed-meter topology, Sagnac and polarization-based speed meters. While speed meters have the radiation pressure noise proportional to f, acceleration meters can make it flat sacrificing its shot noise.
References:

- J. Li, and T. Zhang, Class. Quantum Grav. 39 055007 (2022).

3.10.3 Negative inertia

Version history: First version in 2024 by K.Somiya
Feasibility: 1

The equation of motion of the mirror with an optical spring is basically given by $m\ddot{x} = -kx + F$ with k a spring constant. The response to the external force is enhanced at around $\omega = \sqrt{k/m}$. The narrow band signal enhancement can be realized by introducing a detuned signal recycling to a Michelson interferometer, i.e. a position meter. If we introduce a detuned signal recycling to a Sagnac interferometer, i.e. a speed-meter, the equation of motion is in the form of $m\ddot{(x)} = -k\ddot{x} + F$ since the output field reflected by the signal-recycling mirror is proportional to $\dot{x}$ and the reflected field hits the mirror twice with a time difference. A positive coupling constant k will increase the effective mass. A negative k will decrease the effective mass and enhance the response to the external force in a broad band; this technique is called *negative inertia*. The first version with a detuned signal-recycled Sagnac interferometer was discovered by Müller-Ebhardt and Chen, but the work was not published. Khalili published an alternative method using double optical spring in 2010.

References:

- F.Khalili *et al.*, Phys. Rev. D. 83, 062003 (2018)

3.10.4 Local readout

Version history: First version in 2019 by K.Somiya
Feasibility: 1

With the signal recycling cavity detuned from the resonance or anti-resonance, the four test masses are locked by an optical spring. The 3-km arm cavity then

reacts to the gravitational waves like a mechanical spring to physically move the test mass at and below the spring frequency. Since the ITM moves physically, the motion can be measured by a local probe. This scheme is called a local readout scheme. A differential motion of the ITMs is already measured in the current detectors: the degree of freedom is often called MICH. If we could improve the sensitivity of the MICH measurement and combine the regular gravitational wave channel from the arm cavities, which is often called DARM, the total sensitivity could be improved.

A similar technique was suggested in [Courty 2003]. They proposed to use a local readout to measure the motion of the ETM and cancel quantum radiation pressure noise. The local measurement certainly imposes extra shot noise but the noise level can be lower than radiation pressure noise of the carrier light. This technique is called quantum locking.

A systematic study of the local readout was performed in [Rehbein 2007]. They showed that the sensitivity can be improved with the technique for advanced LIGO.

The original idea of the local readout comes from [Braginsky 1997]. The technique was called the optical bar regime. Khalili proposed to upgrade the optical bar to the optical lever [Khalili 2002]. This idea leads to the intracavity signal amplification techniques proposed by Chen and Somiya in 2012.

References:

- J.-M. Courty1 *et al.*, Europhys. Lett. 63, 226 (2003)
- H. Rehbein *et al.*, Phys. Rev. D, 76, 062002 (2007)
- V. Braginsky *et al.*, Phys. Lett. A, 232, 340 (1997)
- F. Khalili, Phys. Lett. A, 298, 308 (2002)

3.10.5 Photon counting

Version history: First version in 2024 by Y. Nishino.
Feasibility: 2

One alternative readout method is photon counting [arXiv:2211.04016]. In conventional homodyne or heterodyne detection, the detector's sensitivity is limited by quantum shot noise, which originates from the coupling between the local oscillator field and vacuum fluctuations at the same frequency as the signal sideband fields. Instead, by directly counting photons from the signal sidebands at a dark fringe, one can avoid the shot noise. Noise distribution of homodyne detection is Gaussian, while that of photon counting is Poisson with less variance.

References:

- L. McCuller, arXiv:2211.04016.

3.10.6 Delay line

Version history: First version in 2019 by K.Somiya
Feasibility: 4

If the absorption or the inhomogeneity of the sapphire substrate turns out to be a big issue, the delay line technique could be a solution. The delay line does not require a partially transmissive mirror in an arm. In fact, the delay line requires a larger mirror to accommodate many reflection points on one surface, which would be quite challenging.

One realistic way, which would be worth considering for the KAGRA upgrade, is to fold the beam only once in the arm, using the current ETM as a folding mirror and the current ITM as the end mirror. This is the same configuration as GEO. The signal recycling cavity is kept anti-resonance for the carrier light. This broadband signal recycling configuration is not suitable for a high-power operation as the beam power on the beam splitter needs to be high, but this can be good for a low-power operation. Giving up a good transmission in the substrate, an available sapphire could be large. Even an a-axis sapphire or a silicon could be used. Thermal noise of the room-temperature beam splitter could be an issue, but the delay line configuration lowers the influence of the beam splitter by $1/\sqrt{6}$ if the noise level is the same as the test masses. In addition, the fibers of the test masses can be thin for having low absorption compared with input test masses.

3.10.7 Displacement noise free interferometer

Version history: First version in 2024 by A. Nishizawa.
Feasibility: 1 (Theoretically difficult to realise at 100 Hz or below.)

The idea of a displacement noise-free interferometer (DFI) was first proposed in 2004 by [Kawamura & Chen 2004] and was later generalized to the idea canceling both displacement noise and timing noise [Chen & Kawamura 2006], [Chen *et al.* 2006]. In the DFI designs, displacement noise and timing noise are perfectly cancelled, but a GW signal is also cancelled at low frequencies below the characteristic frequency of the DFI, that is , $f_c = c/L$, where L is the characteristic size of the DFI. As a result, the sensitivity to GW amplitude below f_c is at best f^{-2}. For a typical interferometer on the ground, the characteristic size is $L = 3\,\mathrm{km}$ and $f_c = 100\,\mathrm{kHz}$, which is too high for the detection of astrophysical GW sourses. There have been many efforts lowering f_c to 1 Hz, e.g. [Somiya *et al.* 2007], but all the studies failed. The current consensus in the community is that the optical DFI does not improve the sensitivity of the current ground-based detectors such as LVK. It has been shown recently that slow neutrons instead of light can realize a DFI around 1 Hz [Nishizawa *et al.* 2022]. However, a neutron interferometer is beyond the scope of the KAGRA collaboration. A novel theoretical idea for an optical DFI is necessary.
References:

- S. Kawamura and Y. Chen, Phys. Rev. Lett. 93, 211103 (2004).

- Y. Chen and S. Kawamura, Phys. Rev. Lett. 96, 231102 (2006).
- Y. Chen *et al.*, Phys. Rev. Lett. 97, 151103 (2006).
- K. Somiya *et al.*, Phys. Rev. D 76, 022002 (2007).
- A. Nishizawa *et al.*, Phys. Rev. D 105, 124017 (2022).

3.10.8 L resonator

Version history: First version in 2024 by Y. Nishino.
Feasibility: 2

L resonator aims to detect high-frequency ($\sim$ 1 kHz) signals especially from NS-NS merger's ring-down phase [Phys. Rev. X 13, 021019]. By replacing the beam splitter in the conventional Fabry-Pérot Michelson (FPMI) style with a high-reflectivity mirror and flipping its angle by 90 degrees, laser light can resonate inside the arm, sloshing between both arms. By this process, signals at the frequency of the sloshing can be amplified as a synchronous-type interferometer [AIP Conf. Proc. 96, 335 (1983)]. Compared to the dual-recycled FPMIs, L resonator is more robust against loss in the signal extraction cavity.
References:

- T. Zhang, et al., Phys. Rev. X 13, 021019.
- R. Drever, AIP Conf. Proc. 96, 335 (1983).

3.11 Calibration

3.11.1 Multi-color calibration

Version history: First version in 2024 by R. Sugimoto.
Feasibility: 3 (A. Guputa demonstrated with a Caltech 40 m in 2023)

Multi-color calibration (hereafter called Mc-CAL) is a calibration method proposed in Anchal Gupta's PhD thesis in 2023 [A. Gupta, 2023]. In the sense that it requires the excitation of mirror displacement, Mc-CAL is similar to conventional calibrations such as P-CAL or G-CAL. However, whereas the accuracy of conventional calibration methods is reliant on the absolute displacement value of the mirror due to excitation, Mc-CAL makes it possible to measure the displacement value itself from the beat signal between lasers that follow the single main arm cavity and CARM degree of freedom respectively, along with the laser frequency and the length of the interferometer. Therefore, it is not necessary to know the efficiency of the actuator used for excitation. It is even possible to calibrate the actuator for the excitation. According to the estimation in the proposed paper, an accuracy of 0.1 % is expected.

Mc-CAL is mainly considered for LIGO and utilizes a lock acquisition system with a 532 nm auxiliary laser called ALS (Arm Length Stabilization) [K. Izumi, et al. 2012] [A. Staley, et al. 2015] . ALS provides independent frequency locking to the single-arm cavity using a separate auxiliary laser from the 1064 nm

main laser. Suppose that the main laser is locked to the CARM degree of freedom, and the auxiliary laser is locked to the single arm cavity on one side (here, the X arm). Here, we excite the arm by adding displacement modulation to the X arm using a certain method. At this time, the frequency fluctuation of the auxiliary laser that follows the X arm is $G_{\mathrm{AUX\_CL}}(\nu_{\mathrm{AUX}}/L_{\mathrm{X}})\delta L_{\mathrm{X}}$. On the other hand, the frequency fluctuation of the main laser following the CARM is $G_{\mathrm{CARM\_CL}}(\nu_{\mathrm{main}}/L_{\mathrm{C}})\delta L_{\mathrm{C}} = G_{\mathrm{CARM\_CL}}(\nu_{\mathrm{main}}/2L_{\mathrm{X}})\delta L_{\mathrm{X}}$ in the same way. Where, $G_{\mathrm{AUX\_CL}}$ and $G_{\mathrm{CARM\_CL}}$ are the closed-loop transfer functions of the AUX and CARM loops, respectively, ν_{AUX} and ν_{main} are the laser frequencies of the auxiliary and main lasers, and L_{C} is the length of the CARM degree of freedom, defined as $(L_{\mathrm{X}} + L_{\mathrm{Y}})/2$. Then, taking the beat of these two, the frequency fluctuation becomes $\delta\nu_{\mathrm{beat}} = (G_{\mathrm{AUX\_CL}} - G_{\mathrm{CARM\_CL}}/2)(\nu_{\mathrm{main}}/L_{\mathrm{X}})\delta L_{\mathrm{X}}$. Here, we assumed that the beam for taking the beat is obtained from the appropriate part either before or after SHG at the same frequency, and that in ALS, the auxiliary laser is phase-locked to the main laser, making $\nu_{\mathrm{AUX}} \to \nu_{\mathrm{main}}$ within the bandwidth of the phase-locked loop. Thus, due to the difference in the frequency response to arm length variations between the main laser and the auxiliary laser, the excitation signal leaks into the beat frequency fluctuations. Finally, we assume that the displacement caused by the excitation actuator is as follows: $\delta L_{\mathrm{X}} = \Gamma\cos(2\pi f_{\mathrm{ext}}t)$, where f_{ext} is the excitation frequency (i.e. the calibration frequency), and Γ is the efficiency of the excitation actuator we are interested in. At this point, we can obtain Γ by demodulating the acquired beat signal at the excitation frequency and combining it with the laser frequency and cavity length. In this way, Mc-CAL allows for the measurement of the displacement amount regardless of the characteristics of the excitation actuator.

Although KAGRA also has ALS and is essentially a system similar to that of LIGO, there are differences in its configuration [T. Akutsu, et al., 2020] [Y. Enomoto, 2020]. Due to these differences, further consideration is required for the implementation of Mc-CAL in KAGRA. For example, in the case of KAGRA, the frequency of the auxiliary laser is controlled with an AOM, so the beam for the beat must be picked off from downstream of the AOM. In addition, KAGRA does not have an SHG for the main laser like LIGO, because the CARM and DARM signals are generated electronically in KAGRA ALS. However, since no other significant elements are missing, the implementation of Mc-CAL in KAGRA should not be difficult with the addition of an SHG for the main laser, a few additional optical components for beat detection, and equipment for measuring the beat frequency.

References:

- A. Guputa, PhD thesis of California Institute of Technology (2023).
- K. Izumi, et al., J. Opt. Soc. Am. A 29, 2092-2103 (2012).
- A. Staley, PhD thesis of Columbia University (2015).
- T. Akutsu, et al., Class. Quantum Grav. 37 035004 (2020).

- Y. Enomoto, PhD thesis of University of Tokyo (2020).

3.12 Studies to improve the stability

3.12.1 Tidal compensation using geophysics interferometer

3.12.2 Earthquake monitors

4 Possible Upgrade Plans

In 2019, KAGRA Future Planning Committee (FPC) summarized four upgrade plans, *LF*, *40kg*, *FDSQZ* and *HF*, together with a longer term upgrade plan dubbed *Combined*, that can be achieved by combining multiple technologies for the upgrade. To come up with four upgrade plans, FPC considered what could be achieved within around 5 years and 5 Oku-yen. Therefore, FPC considered implementing only single upgrade for each plan, and did not considered any mirror or coating improvements over the design parameters summarized in JGW-T1707038. The change in the ITM transmission was also not considered. Details of each plan can be found in the KAGRA FPC White Paper [JGW-M1909590] and in PRD 102, 022008 (2020).

In this section, we first summarize outstanding issues in the current KAGRA detector to achieve the designed sensitivity. We then consider possible upgrade plans assuming all the requirements for achieving the designed sensitivity were met. We start by briefly reviewing each of FPC 2019's four upgrade plans and consider possible further update for each plan.

4.1 Outstanding issues in current KAGRA detector

Here, we summarize outstanding issues in the current KAGRA detector realize the designed fundamental noises. We basically focus on issues related to thermal noise and cryopayload, as summarized in Table 3, but we stress that other technical noises such as acoustic noises, scattered light noises, control noises of course need to be reduced. Current estimates of optical losses in the interferometer are also summarized. Issues are listed roughly in the order of priority to improve the sensitivity.

4.1.1 Low Q-value of sapphire suspensions

The Q-value of the first violin modes estimated from the spectral peak width was $(1.7 \pm 1.1) \times 10^4$ at 250 K [klog 25080]. At temperatures above 100 K, thermoelastic damping is dominant, and this measurement is consistent with the expectation. At 80 K, it was measured to be 10^4 to 10^5, which was significantly lower than the thermoelastic limit [klog 26113]. Off-site measurements by Shishido et al. [Master Thesis by Shishido] also reported the Q-value in the order of 10^5. Further measurements at lower temperatures would be necessary, but this suggest that sapphire suspensions need to be improved to achieve the designed suspension thermal noise.

Item	Designed value	Current value
Sapphire suspension loss angle	2×10^{-7}	$10^{-5} - 10^{-4}$ at 80 K klog 26113
Sapphire mirror loss angle	1×10^{-8}	1×10^{-6} at 80 K JGW-L2315445
Sapphire blade spring loss angle	7×10^{-7}	3.6×10^{-5} JGW-G1910180
Coating loss angle	$3.0/5.0 \times 10^{-4}$	7.7×10^{-4} at 20 K PRD 109, 102008 (2024)
Sapphire mirror absorption	50 ppm/cm	20–30 ppm for ITM PRApplied 14, 014021 (2020)

Table 3: Summary of parameters critical for achieving the thermal noise of the designed sensitivity. Absorption for the current ITM meets the requirement, but was not very reproducible (see, also, Sec. 3.2.3).

4.1.2 Low Q-value of sapphire mirrors

During the investigations of parametric instability, we found that Q-values of sapphire mirror bulk modes are significantly lower than the designed value. Further investigations such as frequency dependence and temperature dependence are underway to guess the source of the excess mechanical loss. Summary of measurements for each test mass at 80 K and at 250 K for each resonant mode is given at JGW-L2315445 and klog 26904.

4.1.3 Low Q-value of sapphire blade springs

As discussed in Sec 3.4.1, loss angle of sapphire blade springs was measured to be 3.6×10^{-5} in 2016 at Kashiwa, while the designed value is 7×10^{-7} [JGW-G1910180]. Lower limits to the Q-values obtained from KAGRA data were on the order of 10^3 to 10^4, according to klog 25931. Since the designed sensitivity at 10–30 Hz is limited by vertical suspension thermal noise [PRD 97, 102001 (2018)], improving the blade spring is critical for achieving the designed sensitivity, especially at low frequencies. Reducing the resonant frequencies of the blade springs also helps increasing the sensitivity at low frequencies. Fabricating compact a blade spring with a simple shape will require significant R&D.

4.1.4 Coating loss angle

For the designed sensitivity, coating loss angles were assumed to be 3.0×10^{-4} for SiO_2 layers and 5.0×10^{-4} for Ta_2O_2 layers, which were consistent with previous measurements in Japan at 20 K using sapphire disks coated by Japan Aviation Electronics Industry and NAOJ [PRD 74, 022002 (2006), PRD 90, 102004 (2014)]. These measurements showed almost no temperature depen-

dence. However, according to the most recent measurement at University of Toyama using LMA coated sample, a peak of the measured loss angle at around 20 K was found. The local maximum was 7.0×10^{-4} for TiO_2 doped ones and 7.7×10^{-4} for undoped ones [PRD 109, 102008 (2024)]. In-situ measurement of the actual coating thermal noise of the KAGRA interferometer would be crucial to understand the actual behavior of the coating deposited on the current test masses. However, as contributions from mirror substrate loss and coating loss are almost equivalent, the direct measurement will be challenging. The reduction of mirror substrate loss reported above is also required before performing coating thermal noise measurements.

4.1.5 High thermal resistance of cryopayloads

For the designed sensitivity calculations, the platform, the marionette and the intermediate mass were assumed to be at 16 K, and the test mass was assumed to be at 22 K. The thermal resistance between the intermediate mass and the test mass was assumed to be

$$R_{\mathrm{f}} = \left(\frac{N_{\mathrm{f}} \pi d_{\mathrm{f}}^2}{4 l_{\mathrm{f}}} \kappa_{\mathrm{f}}(d_{\mathrm{f}}, T) \right)^{-1} = 5.6 \text{ W/m}, \tag{4}$$

where $N_{\mathrm{f}} = 4$, $d_{\mathrm{f}} = 1.6$ mm, $l_{\mathrm{f}} = 26.1$ cm, $\kappa_{\mathrm{f}} = 5800$ W/m/K (at 20 K for given fiber diameter) are the number of the sapphire fibers, the fiber diameter, the fiber length, and the fiber thermal conductivity, respectively.

In reality, during the cool down test, when the test mass reached 23 K, the intermediate mass, the marionette, the platform were 22 K, 20 K and 20 K, respectively. At that time, cooling bar temperature was 9 K. Considering the heat load at that time, thermal resistance between the cooling bar and the test mass was estimated to be roughly 70 W/K [JGW-G1910636]. This was far more than the requirement, and it was pointed out that reaching 22 K with laser absorption would be impossible [JGW-G1910569]. Further investigations and improvements in the thermal conductivity would be necessary for increasing the laser power while keeping the cryogenic temperatures.

4.1.6 Sapphire mirror birefringence

Due to inhomogeneous birefringence of sapphire ITMs, we are having excess optical losses and contrast defect in the central interferometer. This would lead to lower power recycling gain, unstable interferometer controls and excess laser noise couplings. Currently, we are experiencing up to 10% loss with an ITM single bounce [PRD 110, 082007 (2024)], and a factor of 3 reduction due to Lawrence effect after locking the arms [PRD 109, 022009 (2024)]. See Sec. 3.2.3 for recent progress on producing better sapphire masses.

4.1.7 Optical losses in the interferometer

We also note that optical losses in the interferometer need to be evaluated and compared with the requirements to judge if we can achieve the designed quantum

noise (see Table 4). The arm cavity round-trip loss for each arm was estimated to be around 50 ppm [klog 30823], which is consistent with the estimate from the test mass characterizations reported in PRApplied 14, 014021 (2020) and meets the 100 ppm requirement. The estimate from the measured power recycling gain of 14.5 and X and Y arm finesses of 1300 and 1420, respectively, gives arm cavity round-trip loss of around 78 ppm.

In the sensitivity calculation, total of losses in the output optics from SRM to OMC DC PD is assumed to be 10%. Optical losses of the current output optics can be summarized as follows.

- OFI: 5% [JGW-G1809012, OFI wiki]
- OSTM: 0.89% [klog 30229]
- OMC: 5% [klog 30229]
- DC PD: 7% [Currently using Excelitas C30665GH]

Sum of these already exceeds the 10% requirement. Also, rough estimate from the measured shot noise at KAGRA gives around 15% of total loss. Making phase-2 OFI and OMC, together with installing high quantum efficiency PD would be necessary. The impact to the quantum noise is not significant at this point, but will be for squeezing.

Item	Designed value	Measured value
Arm cavity round-trip loss	100ppm	50–80ppm (see text)
Losses in SRC	0.2%	not measured??
Total losses in output optics	10%	15% (see text)

Table 4: Summary of optical losses assumed in the sensitivity calculations and current estimates.

4.2 Example upgrade plans

Here, we describe possible upgrade plans focusing on low frequency, high frequency and broadband by showing example sensitivity curves. We start by briefly reviewing FPC 2019's upgrade plans and consider possible further update for each plan, and compare it with bKAGRA [JGW-T1707038], aLIGO [LIGO-T1800044], A+ [LIGO-T1800042] and A# [LIGO-T2300041] sensitivity curves (see Fig. 9a).

In FPC 2019's plans, following seven parameters were optimized for specific figure of merit to find the optimal laser power and mirror temperature [PRD 102, 022008 (2020)].

- SRC detuning angle (0 to 3.5 deg; 0 to 60 deg for LF case)
- Homodyne angle (90 to 180 deg)

- Mirror temperature (20 to 30 K)
- Laser power at BS (with an upper limit set by heat extraction capability but not higher than 3500 W considering PSL power available)
- SRM reflectivity (50 to 100 %)
- Sapphire fiber length (20 to 100 cm, considering the size of the inner shield)
- Sapphire fiber diameter (with a lower limit set by a tensile strength to suspend the test mass)

It is worth noting that, changing sapphire fiber length and diameter requires significant R&D, and it takes time to revert the change. The other parameters above are relatively easy to revert the change. Detector parameters for the example upgrade plans discussed in this section are summarized in Table 5.

4.2.1 Low frequency

FPC 2019's *LF* plan in Fig. 9b was made by optimizing the seven parameters to maximize the inspiral range to $100M_{\odot}$-$100M_{\odot}$ binary, under following upgrades to the cryopayload.

- The mass of the intermediate mass is increased by a factor of 4 from 20.5 kg to 82 kg.
- The diameter and length of the CuBe wires suspending the intermediate mass is changed from 0.6 mm in diameter, 26.1 cm in length, to 0.2 mm in diameter, 78.3 cm in length.
- Other than the heat load from the laser power, additional heat introduced to the test mass was reduced from 50 mW to 3 mW.

Since the sensitivity is limited by the vertical suspension thermal noise, further improvement would be possible by reducing the vertical resonant frequency of the blade springs from 14.5 Hz to, for example, 5 Hz [JGW-G2113082], as shown in Fig. 9c. Realizing 5 Hz blade spring will be a challenge, but this will give some more room for quantum noise to improve. Increasing the mirror mass to 40 kg would not help improving the inspiral range much. Although the larger beam can be adopted and it implies the smaller coating thermal noise, the sensitivity is mainly limited by shot noise which could not be reduced dramatically.

However, due to reduced heat extraction capability from longer sapphire fibers, introducing higher laser power would not be possible. In order to fully take advantage of reduced suspension thermal noise, frequency dependent squeezing with a 300-m long, 30 ppm loss filter cavity, 40 kg test masses and a factor of two reduction of lower absorption would be necessary. Sadly, even with these upgrades, sensitivity would only reach the designed sensitivity of A#, as shown in Fig. 9d. The sensitivity curve in Fig. 9d was particle-swarm-optimized to

maximize the inspiral range to $100M_\odot$-$100M_\odot$ binary without the SRC detuning.

This parameter set to realize broadband quantum noise reduction is just an example. To achieve similar quantum noise with a 85-m filter cavity, which is currently considered for the KAGRA Filter Cavity project, round-trip loss of the filter cavity needs to be ppm level. Equivalent broadband reduction could be possible by implementing other quantum control schemes such as variational readout. Improvements in the coating thermal noise with larger beam and coating loss angle reduction would not be very effective for improving *LF* plans.

4.2.2 High frequency

FPC 2019's *HF* plan in Fig. 9e was made by optimizing the seven parameters to maximize the sky localization of GW170817-like binaries all over the sky, under following upgrades.

- Increased limit to power at BS from 1500 W to 3500 W.
- Input frequency independent squeezing of 10 dB (Detected squeezing of 6 dB at maximum).

Further improvement in the sky localization would be possible if the optical loss in SRC is reduced from the designed value of 2000 ppm to 500 ppm, and the optical loss in the inteferometer output chain is reduced from the designed value of 10% to 5%, as shown in Fig. 9f. This plan would lead to the sensitivity equivalent to A# at high frequencies. Intra-cavity power higher than A# could be realized with the cryogenic operation.

Using the long SRC effect, we can create a dip at high frequencies, which enables us to probe into neutron star physics by observing post-merger signals. By reducing the ITM transmission from 0.4% to 0.2% and increasing the SRM reflectivity to 99.5%, a dip at around 2 kHz beyond A# sensitivity can be realized, as shown in Fig. 9g. A dip at around 3 kHz can be created without changing the ITM transmission, as shown in Fig. 9h. To create these sensitivity curves, optical losses were reduced similarly to the plan in Fig. 9f, and the seven parameters were particle-swarm-optimized to maximize the sensitivity at the dip, with a constraint that maximum SRM reflectivity is 99.5%. Reduction of optical losses, high power operations and the lock of high finesse SRC would be technical challenges.

Plans discussed here are similar to the plans in JGW-G2113082, and more recently the plans *HFmod FIS*, *HF2k FIS* and *HF3k FIS* discussed by KAGRA 10yr Task Force [JGW-T2415721]. Here the parameter optimization resulted in shorter and thicker sapphire fibers to allow for more power, but the plans discussed by KAGRA 10yr Task Force incorporate more squeezing without changing the fiber dimensions. Changing the fiber dimensions involve significant R&D, and it takes time to reverse the change. Adjusting the signal recycling configuration and laser power are relatively straightforward changes that can be

reversed, making these adjustments an attractive first step toward broadband sensitivity improvements.

Science case studies revealed that *HFmod* is preferable among these three candidate plans from CW point of view [JGW-T2415830], *HF3k* from event rate estimates of post-merger signals [JGW-G2415992], and *HFmod* from tidal deformability measurements and CBC event rates [JGW-G2416000]. These would imply that the change in the ITM transmission to tune the dip frequency to around 2 kHz is not very necessary. The design studies for NEMO revealed that around $10^{-24}/\sqrt{\mathrm{Hz}}$ sensitivity at 1-3 kHz range is necessary for probing neutron star physics [PASA 37, e047 (2020)], and both Fig. 9g and Fig. 9h meet this requirement.

4.2.3 Broadband

FPC 2019's *40kg* and *FDSQZ* plans in Fig. 10a and Fig. 10b, respectively, were made by optimizing the seven parameters to maximize the inspiral range to $1.4M_\odot$-$1.4M_\odot$ binary, with 40 kg test mass instead of 22.8 kg and with frequency dependent squeezing with a 30-m filter cavity, respectively. *40kg* plan resulted in a detuned configuration to take advantage of the reduced coating thermal noise due to larger beam size, while *FDSQZ* plan resulted in a broadband configuration.

Simply combining 40 kg test masses and frequency dependent squeezing with a 85-m filter cavity would make the sensitivity curve in Fig. 10c, and the improvement over the plans in 2019 is not very significant. Reduction in the optical losses, 300-m filter cavity, and coating thermal noise reduction by a factor of 2 would make the sensitivity curve in Fig. 10d.

To make the most out of frequency dependent squeezing, suspension thermal noise also need to be reduced using technologies considered for *LF*. Further adding low frequency options for suspensions discussed in Sec. 4.2.1 and 5 Hz blade spring will allow for the sensitivity curve in Fig. 10e. This sensitivity curve will be roughly equivalent to A+ sensitivity.

To achieve A# level sensitivity, further increase in the mirror mass to 100 kg, a factor of 4 reduction in the coating thermal noise from the default, a factor of 4 reduction in the absorption, and roughly 4 MW in each arm cavity would be required, as shown in Fig. 10f. All the sensitivity curves in were particle-swarm-optimized to maximize the inspiral range to $1.4M_\odot$-$1.4M_\odot$ binary. Changing the ITM transmission from 0.4% to 0.2% will improve the range by around 2%.

These studies show that, technologies to reduce suspension and coating thermal noise while keeping high power operation are crucial. Those include enhanced thermal conductivity, reduced absorption, reduced mechanical losses, and low-loss optics for more squeezing to reduce quantum noise without increasing the laser power.

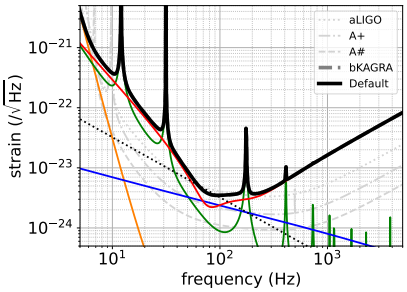

(a) Default bKAGRA

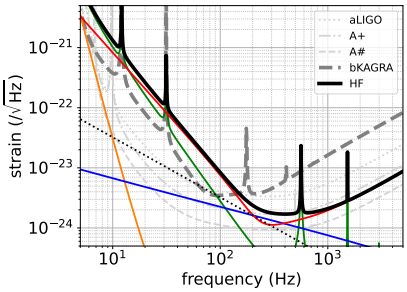

(e) HF 2019

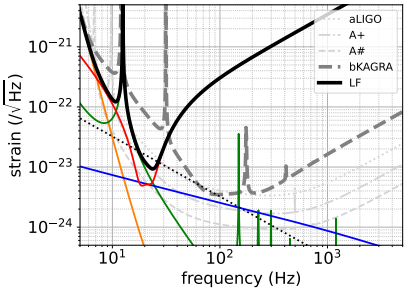

(b) LF 2019

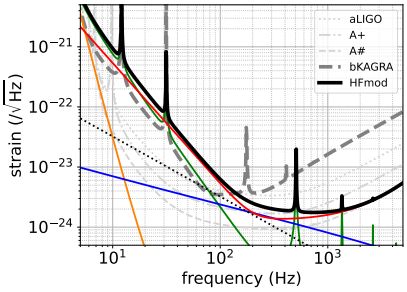

(f) HFmod

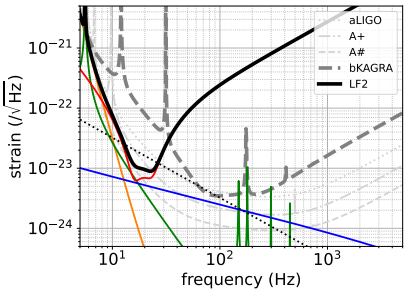

(c) LF2

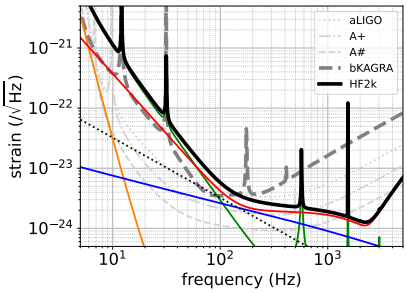

(g) HF2k

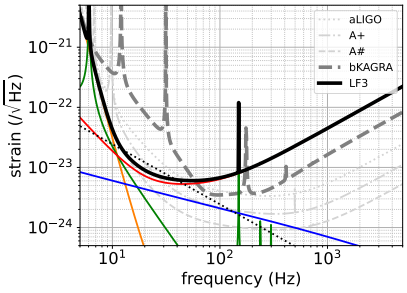

(d) LF3

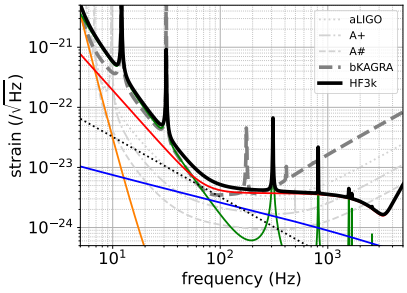

(h) HF3k

Figure 9: Sensitivity curves of various example upgrade plans (part 1).

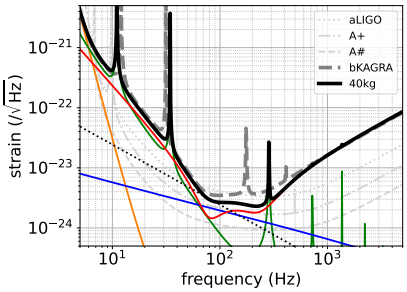

(a) 40kg 2019

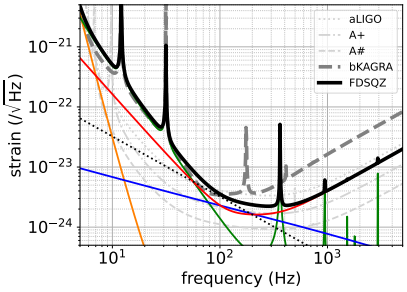

(b) FDSQZ 2019

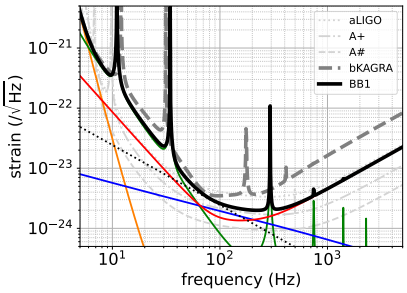

(c) BB1

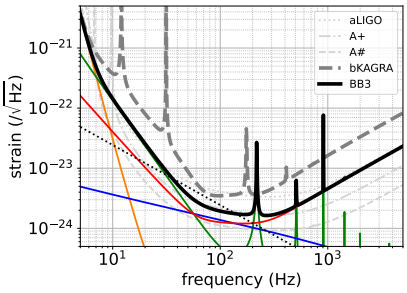

(e) BB3

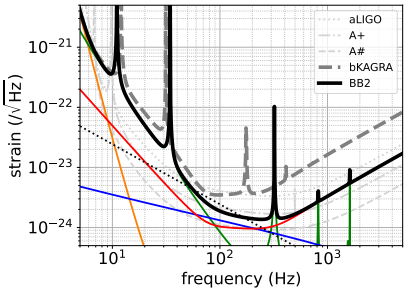

(d) BB2

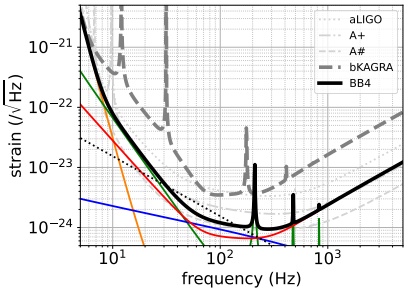

(f) BB4

Figure 10: Sensitivity curves of various example upgrade plans (part 2).

Table 5: Detector parameters for example KAGRA upgrade plans.

	Symbol	Default	LF	LF2	LF3	HF	HFmod	HF2k	HF3k	40kg	FDSQZ	BB1	BB2	BB3	BB4
SRC detuning angle (deg)	$\phi_{\rm det}$	3.5	28.5	29.7	0	0.1	0	0	0	3.5	0.2	0.2	0.1	0.1	0.1
Homodyne angle (deg)	ξ	135.1	133.6	133.3	90	97.1	91.3	90	90.2	123.2	93.1	90.7	90	90	90
Mirror temperature (K)	$T_{\rm m}$	22	23.6	23.1	22.4	20.8	22.2	24.3	24.1	21	21.3	20.9	20.8	21.4	20
Power at BS (W)	I_0	673.6	4.5	3.6	19.8	3398.4	3140.5	3527.9	3505.7	1509.7	1518.8	1507.8	1470.0	790.2	2879.6
SRM reflectivity (%)	$R_{\rm SRM}$	84.64	95.5	90.7	51.1	90.7	95.6	99.5	99.5	92.2	83.2	80	82.5	79.8	82.9
Sapphire fiber length (cm)	l_3	35	99.8	100	100	20.1	20	20	26.6	28.6	23	28.2	26.6	33.2	40.2
Sapphire fiber diameter (mm)	d_2	1.6	0.5	0.5	0.6	2.5	2.1	2.5	2.2	2.2	1.9	2.2	2.2	1.8	2.3
Mirror mass (kg)	m	22.8	22.8	22.8	40	22.8	22.8	22.8	22.8	40	22.8	40	40	40	100
Beam radius (mm)	w_2	35.0	35.0	35.0	42.2	35.0	35.0	35.0	35.0	42.2	35.0	42.2	42.2	42.2	57.3
FC length (m)	$L_{\rm fc}$	0	0	0	300	0	0	0	0	0	30	85	300	300	300
Maximum detected squeezing (dB)	$\sigma_{\rm maxSQZ}$	0.0	0.0	0.0	7.4	6.1	7.2	7.2	7.3	0.0	5.2	5.3	9.1	9.0	9.0
ITM transmission (%)	$T_{\rm ITM}$	0.4	0.4	0.4	0.4	0.4	0.4	0.2	0.4	0.4	0.4	0.4	0.4	0.4	0.4
Arm cavity round-trip loss (ppm)	$\Lambda_{\rm rt}$	100	100	100	100	100	100	100	100	100	100	100	100	100	100
SRC loss (ppm)	$\Lambda_{\rm SR}$	2000	2000	2000	500	2000	500	500	500	2000	2000	2000	500	500	500
PD loss (%)	$\Lambda_{\rm out}$	10	10	10	5	10	5	5	5	10	10	10	5	5	5
Injection losses (%)	$\Lambda_{\rm inj}$	5	5	5	2	5	5	5	5	5	5	5	2	2	2
FC round-trip loss (ppm)	$\Lambda_{\rm fc}$	0	0	0	30	0	0	0	0	0	30	30	30	30	30
Readout loss (%)	$\Lambda_{\rm ro}$	0	0	0	2	0	0	0	0	0	5	5	2	2	2
Coating loss angle 1 (1e-4)	$\phi_{\rm c1}$	3	3	3	3	3	3	3	3	3	3	3	0.75	0.75	0.1875
Coating loss angle 2 (1e-4)	$\phi_{\rm c2}$	5	5	5	5	5	5	5	5	5	5	5	1.25	1.25	0.3125
IM mass (kg)	m_1	20.5	82	82	82	20.5	20.5	20.5	20.5	20.5	20.5	20.5	20.5	82	82
IM wire length (cm)	l_1	26.1	78.3	78.3	78.3	26.1	26.1	26.1	26.1	26.1	26.1	26.1	26.1	78.3	78.3
IM wire diameter (mm)	d_1	0.6	0.2	0.2	0.2	0.6	0.6	0.6	0.6	0.6	0.6	0.6	0.6	0.2	0.2
Blade spring vertical resonance (Hz)	$f_{\rm mg}$	14.5	14.5	5	5	14.5	14.5	14.5	14.5	14.5	14.5	14.5	14.5	0.5	0.5
Substrate absorption (ppm/cm)	$\beta_{\rm m}$	50	50	50	25	50	50	50	50	50	50	50	50	50	12.5
Coating absorption (ppm)	$\beta_{\rm c}$	0.5	0.5	0.5	0.25	0.5	0.5	0.5	0.5	0.5	0.5	0.5	0.5	0.5	0.125
Additional heat (mW)	$P_{\rm amb}$	50	3	3	3	50	50	50	50	50	50	50	50	3	3
$100-100M_\odot$ inspiral range (Mpc)		353	2019	3516	3787	112	158	146	269	400	306	542	552	1142	2154
$30-30M_\odot$ inspiral range (Mpc)		1095	1088	1525	2382	270	388	424	705	1250	842	1377	1665	2487	4229
$1.4-1.4M_\odot$ inspiral range (Mpc)		153	85	119	196	155	156	141	117	202	178	229	313	320	537
Sensitivity at dip (1/rtHz)		3.5e-24	9.3e-24	8.9e-24	6.0e-24	1.7e-24	1.8e-24	1.3e-24	1.6e-24	2.3e-24	2.2e-24	2.0e-24	1.4e-24	1.6e-24	9.4e-25